# EFFECTIVENESS ANALYSIS OF SLOTTED ORIFICE PLATE MULTIPHASE FLOW METER COUPLED WITH VENTURI METER AND VISUALIZATION STUDY

A Thesis

by

KE LI

Submitted to the Office of Graduate and Professional Studies of
Texas A&M University
in partial fulfillment of the requirements for the degree of

MASTER OF SCIENCE

| | |
|---|---|
| Chair of Committee, | Gerald L. Morrison |
| Committee Members, | Debjyoti Banerjee |
| | Karen Vierow |
| Head of Department, | Andreas A. Polycarpou |

December 2016

Major Subject: Mechanical Engineering

# ABSTRACT

Multiphase flow is a common flow when oil and gas are produced from underground, and in the process of hydrocarbon products transportation. Multiphase flow meters have been one of the most important developments in oil and gas industries. The purpose of inventing a multiphase flow meter is to measure the flow rate of a fluid with multiple phases and/or the fraction of different components in the multiphase fluid.

Electrical impedance measurement is a method that has been recently applied so that a new type of multiphase flow meter can be developed. Its principle is to record instantaneous measurements of impedance of a multiphase fluid. After comparing it to the impedance of each component of the fluid, the fractions of each component are known.

One of the limitations of this method is that the multiphase flow needs to be well homogenized so that the measurement of impedance is accurate and steady. Therefore, in this study a slotted orifice plate is used to homogenize the multiphase flow.

Venturi meters are commonly used to measure the flow rate of a fluid. It uses a converging section of pipe to increase the velocity of the flow which causes pressure drop according to Bernoulli's theory. Flow rate can be calculated when the differential pressure is measured.

Flow visualization is a method to get qualitative or quantitative information of a flow by making the flow patterns visible.

In this research, flow rate and gas volume fraction of a water and gas flow is measures by a slotted orifice plate flow meter coupled with a Venturi meter in different orientations. Electrical impedance measurement method is used to obtain the Gas Volume

Fraction of the working fluid. Results show that the gains of the signals at 1 MHz frequency have $6^{th}$ order polynomial correlations with GVF values in both horizontal and vertical orientations, and that phase angles of the signals at 10 MHz frequency have linear correlations with GVF values only in horizontal orientation. The Venturi meter is used to measure the bulk flow rates of the working fluid. The Discharge Coefficients of the Venturi meter is calculated to be 0.97 and 0.89 in horizontal and vertical orientations respectively. In addition, the Discharge Coefficient of the slotted orifice plate is proved to be independent from orientations. At last, a flow visualization study is conducted to show different flow patterns as well as the homogenization ability of the slotted orifice plate. Results of the visualization study show that the slotted orifice plate has remarkable ability to homogenize the water-air mixture in all flow regimes and in both horizontal and vertical orientations.

# DEDICATION

This thesis is dedicated to my beloved parents, Xuemei Li and Shixin Li. Thank you for your supports when I was at the lowest point of my life, and letting me know there was always hope. I love you! You are the best parents!

This thesis is also dedicated to the cutest girlfriend, Mengqiao Liu. Meeting you has used all my luck in my life, and I will spend my entire life loving you.

# ACKNOWLEDGEMENTS

Special thanks to my advisor, Dr. Gerald. L. Morrison for his instructions, advises, supports and patience throughout this project. It is always fun to learn things from him and I really enjoy working with him. I would also like to thank my committee members, Dr. Karen Vierow and Dr. Debjyoti Banerjee for their supports.

Thanks also go to my best friend and my high school classmate Xi Chen for his company and care. I also want to express my gratitude to all my friends I made in College Station and all my colleagues at Turbomachinery Laboratory.

Finally, thanks to Texas A&M University for the excellent academic environment. It has always been enjoyment to study and live here.

# NOMENCLATURE

| | |
|---|---|
| $\alpha$ | Area ratio of Slotted Orifice Plate |
| $\beta$ | Beta ratio of Venturi pipe |
| $\rho_{air}$ | Air density |
| $\rho_{mix}$ | Mixture density |
| $\rho_{water}$ | Water density |
| A | Cross-sectional area |
| ACFM | Actual cubic feet per minute |
| $C_d$ | Discharge coefficient |
| $C_f$ | Feedback capacitance |
| $C_s$ | Stray capacitance |
| $C_x$ | Capacitance of mixture |
| D | Diameter |
| f | Frequency |
| G | Gain |
| G’ | Modified gain |
| GPM | Gallon per minute |
| GVF | Gas volume fraction |
| P | Pressure |
| $\Delta P$ | Pressure difference |
| $\dot{Q}$ | Bulk volumetric flow rate |

| | |
|---|---|
| $\dot{Q}_{air}$ | Air volumetric flow rate |
| $\dot{Q}_{water}$ | Water volumetric flow rate |
| R | Specific gas constant |
| $R_f$ | Feedback resistance |
| $R_x$ | Mixture resistance |
| T | Temperature |
| $V_i$ | Excitation voltage |
| $V_o$ | Output voltage |
| X | Quality |
| $Z_x$ | Mixture impedance |

# TABLE OF CONTENT

Page

# LIST OF FIGURES

Page

# LIST OF TABLES

Page

# LIST OF VIDEOS

Page

# 1 INTRODUCTION

Multiphase flow is a very common flow when oil and gas are extracted from underground, and in the process of hydrocarbon products transportation. One of the most commonly used methods is to use gravity to separate the multiphase flow into several single-phase flows due to density difference. In such a system, many types of conventional single-phase flow meters can be used, including but not limited to turbine flow meter, Corriolis flow meter, Venturi meter, etc. Conventional separating systems have many disadvantages such as high purchasing and maintenance cost, taking large spaces and requiring a period of time to stabilize in order to increase accuracy. [1] Take water-air flow for example. When fractions of both air and water need to be known instantaneously, several single-phase flow meters with different working ranges are usually used. High measuring accuracy cannot be assured because of different responding time and accuracies of each flow meter. That is to say, when several single-phase flow meters are used together, disadvantages multiply. In the oil and gas industry, especially as it develops more and more economically, metering individual components of oil, water and gas stream is a growing demand. [2]

There are many different designs of multiphase flow meters on the market. Instead of using separators, all multiphase flow meters follow the same principle of measuring the bulk flow rate of the multiphase mixture, calculating the fraction of each phase component, and using these to obtain individual flow rates. [2] Multiphase flow meter usually operates for flows in all flow regimes, providing adequate accuracy and requiring very short responding time.

Twenty years ago, the slotted orifice flow meter was developed in Turbomachinery Laboratory at Texas A&M University. [3] Differing from a standard orifice flow meter which has a single central hole, the slotted orifice flow meter has several arranged radial slots.

The goal of this research is to verify the effectiveness of a slotted orifice flow meter coupled with a Venturi meter and an electrical impedance device with different orientations. And to analyze the homogenize ability of the slotted orifice plate using visualization study.

# 2 LITERATURE REVIEW

The review of literature is important because it shows the originality and relevance of this research topic and it shows what developments have been made based on earlier researches. In this section, the basic information of flow regimes, standard orifice plate, slotted orifice plate, electrical impedance and Venturi meter will be introduced.

## 2.1 Flow Regimes

Flow regimes, or flow patterns are one of the most difficult parts of dealing with multiphase flows. There are so many challenges in understanding, predicting and modeling because a multiphase flow can act in many different forms. [4] In the case of air-water flow, the gas can be seen as small bubbles flowing in water when there is only small amount of air and water flows sufficiently fast. Or, it may appear that little droplets of water are carried by streaming air. [5] Properties of the flow (temperature, pressure, working fluid properties, flow rate, etc.) and properties of the pipe (geometry, size, roughness, bending angle, etc.) can both affect the pattern of the flow. [5]

Even though it is difficult, many researches have been conducted in order to quantitatively describe and predict flow regimes. One of the most popular methods is direct observation by making pipes transparent. For a horizontal gas-liquid flow through a pipe, flow regimes can be generally classified as below and shown in Figure 2.1 in the order of increasing gas flow rate. [6]

– Bubbly flow: occurs when the liquid flow rate is sufficiently high to break up the gas into bubbles, but it is not high enough to let the bubble be mixed well within

the liquid phase. [7] Due to buoyancy force, bubbles are mostly concentrated in the upper half of the pipe. But when shear force dominants, the bubbles tend to disperse in the pipe uniformly. [8]

– Plug flow: gas bubbles are elongated and separate liquid plugs. The diameter of the pipe is larger than the bubbles so that the liquid phase is still continuous along the bottom of the pipe. [8]
– Stratified flow: liquid stays on the lower part of the pipe and gas stays on the upper part. Gas and liquid interface is relatively smooth.
– Wavy flow: amplitude of ripples increase causing waves with notable amplitude. But their crests do not reach the top of the pipe. [8]
– Slug flow: amplitude of waves is high enough to reach the top of the pipe, with some portion of the waves breaking up into bubbles.
– Annular flow: around the perimeter of the pipe, the liquid can form a continuous annular film, and the liquid film is thinner at the top than the bottom. Small amplitude waves disturb the interface between the liquid annular and gas core. Liquid droplets may be dispersed in the gas core. [8]

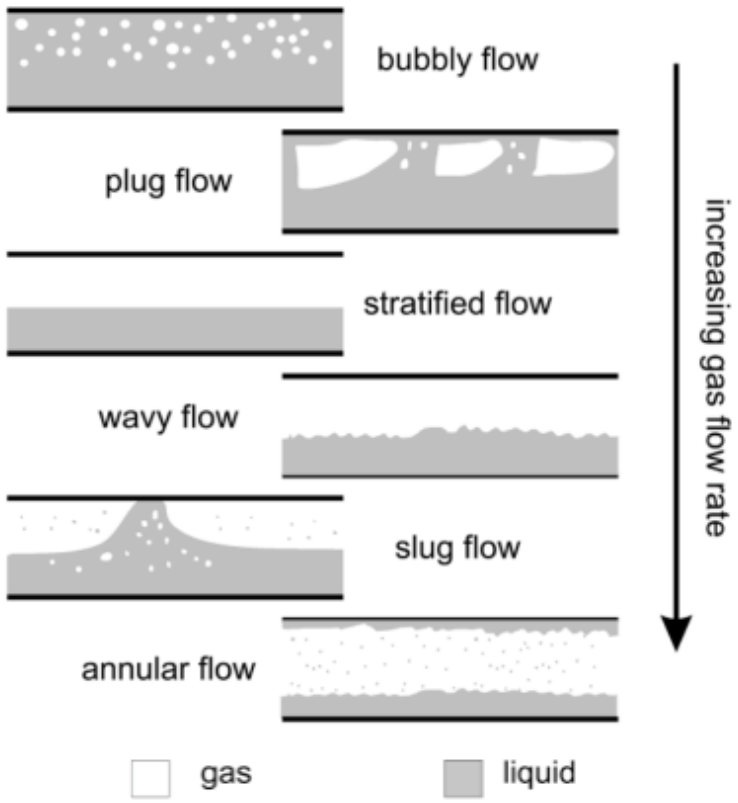


Figure 2.1 Flow regimes in horizontal gas-liquid flows [6]

For a vertical gas and liquid flow downward in a pipe, flows are generally classified into the regimes shown in Figure 2.2 in the order of increasing gas flow rate [6].

– Bubbly flow: liquid is continuous and dispersed gas bubbles can be observed. The bubbles are mostly nearly spherical and much smaller than the size of the pipe. [8]
– Slug flow: bubbles collide with each other and form larger bubbles. Slugs of liquid are separate large bubbles has similar size to the pipe. There is a very thin film of liquid between the large bubbles and pipe wall. [8]

– Churn flow: flow get unstable in the structure. Fluid has a churning motion with a net downward flow rate.

– Annular flow: liquid is driven from the center of the pipe, forming a thin layer on the wall of the pipe with high frequency waves. Liquid droplet may exist in the gas core. [8]

– Mist flow: gas is continuous with liquid exist in the form of droplets.

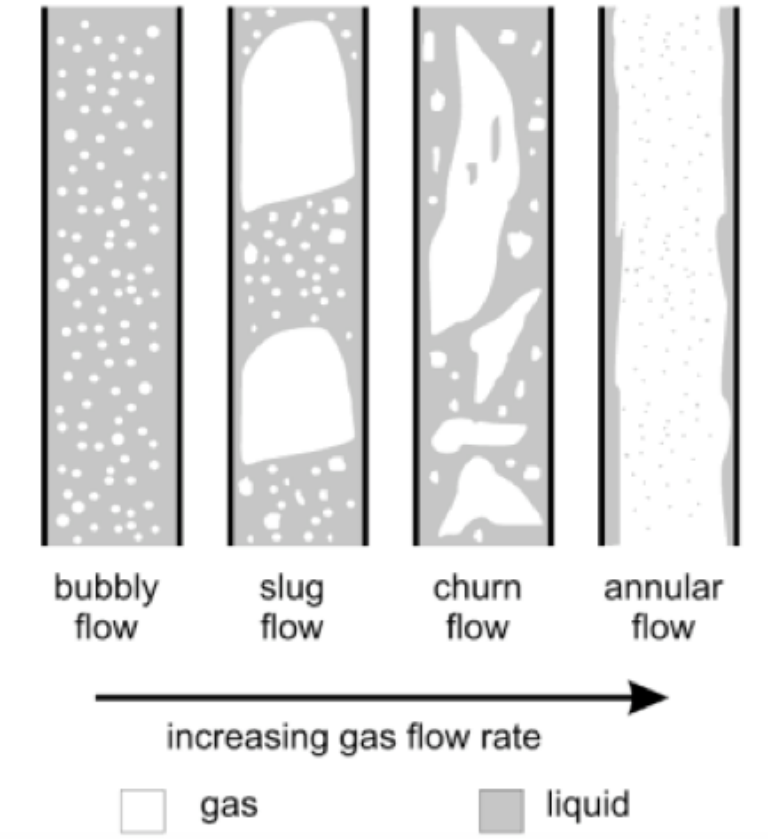


Figure 2.2 Flow regimes in vertical gas-liquid flows [6]

Changing of flow regimes are considered to be functions of two variables, superficial liquid velocity and superficial gas velocity which are both defined to be volumetric flow rate of one phase per cross-sectional area. Then flow regimes can be plotted in maps built with these two variables, and they are called flow regime maps. Figure 2.3 is a flow pattern map for horizontal pipe flows and Figure 2.4 is for vertical pipe flows.

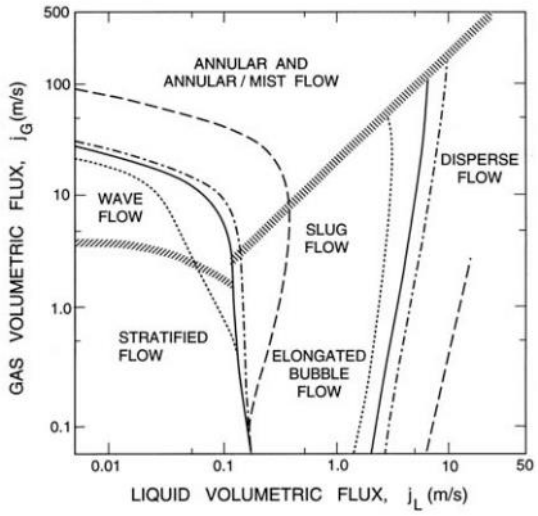


Figure 2.3 Flow pattern map for horizontal pipe flows. From Mandhane et al. (1974). [9]

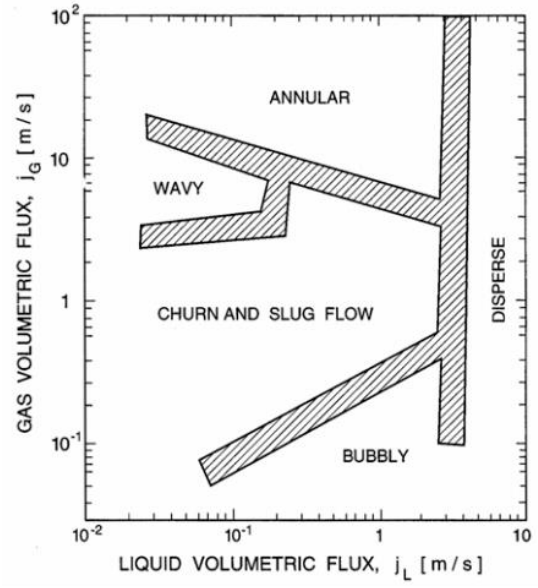


Figure 2.4 Flow pattern map for vertical pipe flow. From Weisman, J. (1983) [10]

## 2.2 Standard Orifice Plate

Differential pressure flow meter is one of the numerous types of flow meters. The orifice plate flow meter is one of the most commonly used differential pressure flow meter. The main principle is to use a plate with a central circular hole to cause pressure difference. [11] [12]

Because of its sensitivity to conditions of upstream flow, the standard orifice plate is required to keep the level of uncertainty below 0.5%. Change of beta ratio ($\beta$), swirl induced by fittings and distance of bend may change the constraint of its level of uncertainty. In ISO 5167-1, there lists standard pipe lengths for upstream and downstream in order to use a standard orifice plate flow meter. [5] In spite of the fact that standard orifice plate flow meter is easy to install and used with low maintenance cost,

disadvantages are quite obvious for the pressure difference being a non-linear function of flow rate and small metering range with normal instrumentations. [13]

## 2.3 Slotted Orifice Plate

The slotted orifice plate was initially used to induce pressure drop and recover the pressure without electrical devices for fluid sampling purposes. Ihfe [14] under the supervision of his advisor Dr. G. L. Morrison, started researches of using slotted orifice plate as a flow conditioner to have a turbulent flow fully developed. However, results indicated that due to high head loss, the slotted orifice plate did not work well as a flow conditioner.

Macek [15], along with Dr. Morrison began investigating the use of slotted orifice plate as part of a single-phase flow meter. The slotted orifice plate turned out to be superior to the standard ones because it had lower overall headloss, less sensitivity to upstream conditions and faster pressure recovery. [15]

Terracina [16] investigated further with Dr. Morrison numerically and experimentally in terms of effecting factors in single-phase measurement, such as mass flow rate, pressure, diameter of pipe, etc. Terracina concluded that when the thickness ratio of the slotted orifice plate was maintained at 0.25, it performed more accurately than the standard orifice plate, because it had much lower discharge coefficient variation for the same beta ratio. [16]

Brewer [17] conducted studies with Dr. Morrison on the performance of the slotted orifice plate in two-phase flows with various flow qualities and a range of beta ratios from

0.43 to 0.5. He found the slotted orifice plate had much faster pressure recovery than standard orifice plate and 2.5 times of pipe diameters upstream and downstream from the plate were the best locations to measure the pressure difference. [17]

Flores [18] repeated the experimental study to determine the performance of slotted orifice plate as a two-phase flow meter under the instruction of Dr. Morrison. She used water and steam as working fluid and compared results with the ones previously obtain from other studies. She found that the pressure difference could be affected by Reynolds number and quality, and uncertainties were primarily contributed by beta ratio. [18]

Sparks [19] carries out studies on comparing mixing abilities of standard and slotted orifice plates, which turned out that slotted orifice plate was superior. She also concluded that thanks to its insensitivity to upstream flow conditions, only a clear pipe with length of 5 times of diameter was needed for the flow meter rather than 10 times that was earlier proposed, and another pipe with the same 5-diameter length was needed for the pressure to recovery.

Cevik [20] compared the slotted orifice flow meter with electrical impedance measurement and swirl-meter on the same working conditions (GVF, water flow rate, and pressure). Experiments showed that slotted orifice plate could provide well-homogenized downstream flow despite the upstream flow conditions, which assured accurate electrical impedance measurement. He also used signals at ten different frequencies and placed six electrode probes at different distance downstream from the slotted orifice and found the

best working signal frequency and the best distance to place electrode probes for a 100 kHz signal were 12 inches on the left coupled with 10 inches on the right respectively.

## 2.4 Electrical Impedance

Since different fluids have different electrical properties and fluids can be classified based on electrical properties, electrical impedance measurement can be used to meter fluids. This techniques measure impedance which describes both resistance and capacitance of a fluid mixture and obtain fractions of each components by comparing the impedance to standard values of the components. [6] One limitation of this technique is that the impedance measurement can be different for different flow regimes. [1]

Fossa [20] conducted experiments to determine the performance of two types of conductance probes in measuring the liquid fraction in a two-phase flow for different flow regimes. He discovered that the ring electrodes had good repeatability in measurements and relatively more flexibility. And for annular flow, the plate electrodes had more sensitivity than the ring electrodes but with greater uncertainty. [20]

Andreussi [21] verified the effectiveness of impedance measurement technique in two-phase gas-liquid flows. Based on experimental results, the impedance method was proved to be effective and convenient. He also found that placing the electrodes between 1.5 and 2.5 times of pipe diameter yielded good results. [21]

Da Silva [6] investigated three different types of impedance sensor that could be used in the electrical impedance technique, complex permittivity needle probe, capacitance wire-mesh sensor, and planar array sensor. He analyzed each sensor system,

indications to measurement uncertainty, advantages and disadvantages, and some specific applications for each type of impedance sensor.

## 2.5 Venturi Meter

Venturi meter has a long history and it has been used in many applications since it was first invented by Giovanni Battista Venturi, an 18$^{th}$-century Italian physicist. Thanks to its reliability and simplicity, Venturi meter has become one of the most common flow meters. Without any abrupt flow restrictions or moving parts, the Venturi meter can provide accurate flow rate measurements with minimal pressure losses. [22]

The basic principle that all Venturi meters follow is the Bernoulli Effect. When a fluid flows through the throat of a Venturi meter where the cross-sectional area is reduced, the fluid speeds up and its pressure declines. Flow rate can be calculated when the pressures at the entrance and throat of the Venturi meter are given. The Bernoulli's equation is stated below.

$$P_1 + \tfrac{1}{2}\rho v_1^2 + \rho g h_1 = P_2 + \tfrac{1}{2}\rho v_2^2 + \rho g h_2 \qquad (2.1)$$

Brook [23] maybe was the first one to investigate the effect of solid-liquid mixture flow in Venturi. He investigated three different methods of measuring velocity and concentration of liquid-solid mixture. He found the Venturi meter being the most accurate method to measure velocity and the best position being vertical.

Graf [24] did experiments on a horizontally place Venturi meter with sand and water mixture. He plotted the correlations of pressure drop against flow rate and modified loss against sediment concentration. He found that it was shown both theoretically and

experimentally that the pressure drop provided information on the flow rate. He also found a correlation between the energy loss and the concentration of the mixture. [24]

Robinson et al [25] carried out experiments for the application of a Venturi meter with various solid concentrations in the working fluid. He used two Venturi meters with different diameters and correlated pressure drop with velocity of working fluid at the throat of Venturi meter and mixture discharge. Two generalized expressions were concluded. $A_m = C_m Q_m^2$ where $A_m$ was the pressure drop of the mixture and $Q_m$ was the mass flow rate. And equation $\frac{b-b_0}{b_0} = kC^n$ related the solid concentration to the relative energy loss, where $k$ and $n$ were determine experimentally. [25]

Shook and Masliyah [26] conducted studies to theoretically and experimentally analyze the affecting factors of slurries flowing through a Venturi meter. They found that discharge coefficients were the greatest contributor rather than wall friction coefficients, and wall friction increased as particle density and size increased. [26]

Herringe [27] studied the behavior of pressure difference for Venturi meter when measuring slurry flow rates and concentration by varying the size of both sand and slurry particles. He also analyzed the performance of Venturi meter in terms of concentration values and discharge coefficient. It was found that only water calibrations were needed for fine slurries while discharge coefficient varied down with the increase of Reynold's number and concentration of solid for coarser slurries.[27]

Hasan et al [28] carried out studies to verify the effectiveness to meter slurries with Venturi meters. Slurries that had low Reynold's number were concluded difficult to measure with Venturi meters for the difficulty to take data, and for high Reynold's number

slurries, discharge coefficients were found having no dependency on Reynold's number, concentration of slurry or throat diameter of the Venturi meter.[28]

Shook [29] conducted an experiment on slurries flowing through Venturi meter horizontally in the stratified regime. He found that compared to discharge coefficient of homogeneous fluids, the discharge coefficient for stratified slurries was even higher, but no quantitative conclusion or prediction was provided. [29]

Kappor et al [30] carried out an experiment to study the application of orifice meter in sediment laden flows by varying the sediment concentration from 0.5% to 7%, finding that for sediment laden flow, the coefficient of discharge was less than that of clear water.[30]

Tiwali [31] investigated behavior of segmental orifice plates whose area ratio varied from 0.143 to 0.625 with clear water and solid water mixture as working fluid respectively. The results indicated that under a limit of Reynold's number, discharge coefficient increases along with the increase of Reynold's number; beyond the limit of Reynold's number, discharge coefficient is only dependent on area ratio. And as the concentration of solid increased, the limiting value of discharge coefficient decreased.[31]

Azzopardi et al [32] investigated the derivation of a quasi-one-dimension model for solid and gas flow in a Venturi meter. The model revealed the change of boundary layer thickness and also acceleration and deceleration of solid and gas particles. This model was validated with previous study results and agreed well.[32]

Bharani et al [33] conducted a study to modify Venturi meters to reduce the erosion rate when flowing solid-liquid mixtures. They calculated discharge coefficients for

various flow conditions and solid concentrations. It was found that there was a small decrease for discharge coefficient after the Venturi meter modification.[33]

Miller et al [34] analyzed the performance of the Venturi meter with emulsion mixture as the working fluid, and derived an equation for discharge coefficient calculation for fluids with Reynold's number between 400 and 24000 with the uncertainty below 6%.[34]

Hollingshead et al [35] carried out an experimental study to analyze the performance of discharge coefficient for Venturi meter, standard orifice meter, wedge flow meter and V cone under both laminar and turbulent flow conditions. It was found that discharge coefficient could be related to Reynold's number after solving the steady Reynold-averaged Navier-Stokes equation with Computational Fluid Dynamics (CFD) method, and it validated with the results from previous experiments. Another conclusion was that for Venturi meter, wedge flow meter and V cone, discharge coefficient increased rapidly along with the increase of Reynold's number when Reynold's number is low. But for orifice meter, before a maximum value was reached, discharge coefficient increased as Reynold's number decreased. The last conclusion was that all four types of flow meters generally show reasonable discharge coefficients for high to moderate Reynold's number, but modification was needed for low Reynold's number flow measurement.[35]

Sihombing [36] studied the temperature effect in multiphase flow meter using Slotted Orifice Plate with air-water mixture being the working fluid and analyzed the homogenization ability of the Slotted Orifice Plate by taking videos and comparing the flow patterns of the upstream and downstream flows. He found that temperature has a

linear effect on signal gain, and introduced a new parameter to eliminate the temperature effect. He found that the most accurate measured GVF is obtained using 1MHz signal, and with the frequency increased, the accuracy decreased.

# 3 GOAL AND OBJECTIVE

The primary goals of this study are:

- Verify the effectiveness of slotted orifice plate flow meter using electrical impedance measurement method coupled with Venturi meter with different orientation
- Analyze the homogenization ability of the slotted orifice plate.

The objectives of this study are:

- Derive the relationships between measured gains and GVFs
- Calculate the bulk mass flow rate
- Calculate the mass flow rate for air and water respectively
- Determine the accuracy of the coupled multiphase flow meter
- Compare the results for different orientations of the flow meter
- Analyze the homogenize ability of the slotted orifice plate
- Determine the most homogenized spot and compare the result to the one from previous experiment
- Compare the homogenize ability of the slotted orifice plate for different flow patterns.

# 4 EXPERIMENTAL FACILITIES AND METHODS

This section introduces all experimental facilities and methods to carry out this study, including primary principles, experimental setups, data acquisitions and analysis.

## 4.1 Experimental Facilities

The experiments were conducted in Test Cell 139, Turbomachinery Laboratory, Texas A&M University. The experimental facilities system can be divided into three parts: water supply system, air supply system, and measurement system. A flow diagram of the facilities is shown in Figure 4.1.

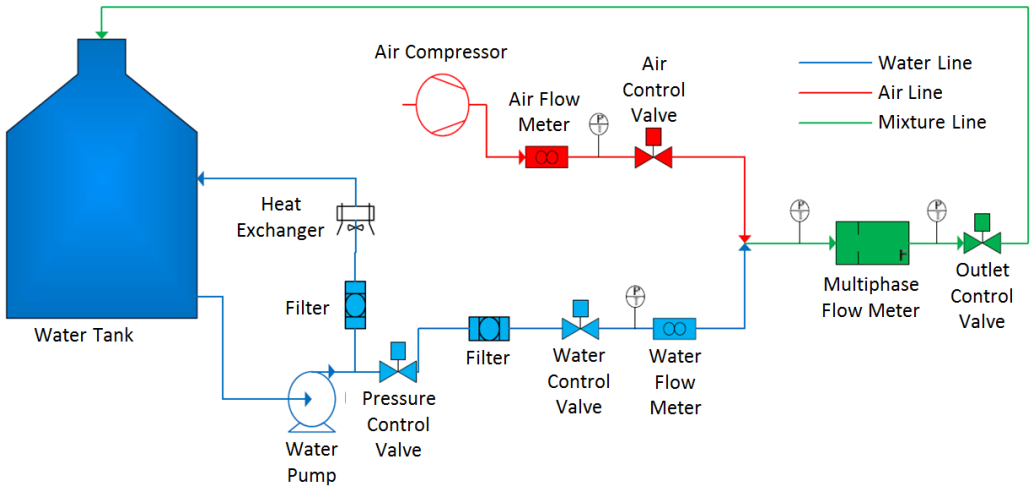


Figure 4.1 Flow diagram of experimental facilities

### 4.1.1 Water Supply System

A fiberglass tank with 5000-gallon capacity is used as a reservoir in the water supply system. Water was pumped out by a centrifugal pump that has 100 Gallon per minute (GPM) capacity from the bottom of the tank. A pressure control valve is installed to keep the water under a maximum pressure of 110 psi. After being filtered, the water flows through three pipes with diameters of 0.5, 1, and 2 inches, where the water flow rate in each pipe is metered by a turbine flow meter that generates electrical pulses whose frequency is directly proportional to the rate of flow. Specifications of the three turbine meters are listed in Table 4.1. The flow rate in each pipe is controlled by a Masoneilan pneumatic butterfly value manufactured by General Electric Company. The open angle of the butterfly value is directly proportional to the 4-20 mA electrical input that is controlled by proportional-integral-derivative (PID) controllers from a LabView program, with fully opening at 20 mA and fully closing at 4 mA input.

Table 4.1 Specifications of turbine meters in water line

| Pipe Size (inch) | Manufacturer | Model | Pulse/Gallon K-factor | Range (GPM) | Uncertainty |
|---|---|---|---|---|---|
| 0.5 | Omega Engineering | FTB-1422 | 13,000 | 0.75-7.5 | 1% |
| 1 | Omega Engineering | FTB-1425 | 911.5 | 5-50 | 1% |
| 2 | Danial Measurement and Control | 1503-1D | 116.5 | 30-300 | 1% |

In the other by-passing water line other than the one with the pressure control valve, a heat exchanger is installed to prevent the water temperature from rising too fast. Before water goes back to the top of the tank, there is a fourth pneumatic value used to control the water pressure during experiments. Figure 4.2 is a flow diagram of water supply system.

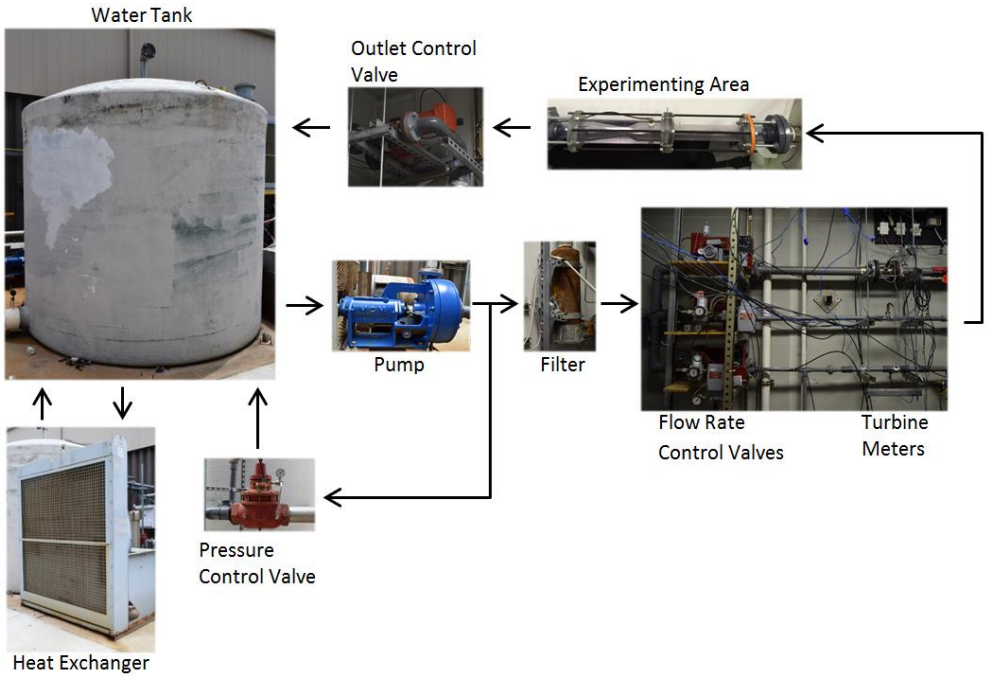


Figure 4.2 Flow diagram of water supply system

### 4.1.2 Air Supply System

Oil-free shop air at a pressure of 110 psi is brought to the system through a 4-inch pipe. Air flow rate is controlled by a Masoneilan pneumatic butterfly value after the air goes through three pipes with diameters of 0.5, 0.5, and 2 inches. Three turbine meters are

installed to measure the volumetric flow rates of the air. Specifications of turbines meters are listed in Table 4.2, and Figure 4.3 is a flow diagram of air supply system.

Table 4.2 Specifications of turbine meters in air line

| Pipe Size (inch) | Manufacturer | Model | Pulse/Gallon K-factor | Range (ACFM) | Uncertainty |
|---|---|---|---|---|---|
| 0.5 | Omega Engineering | FTB-931B | 29749.5 | 0.35-3.5 | 1% |
| 0.5 | Omega Engineering | FTB-933 | 13532.6 | 1-10 | 1% |
| 2 | Omega Engineering | FTB-937 | 629.5 | 6-100 | 1% |

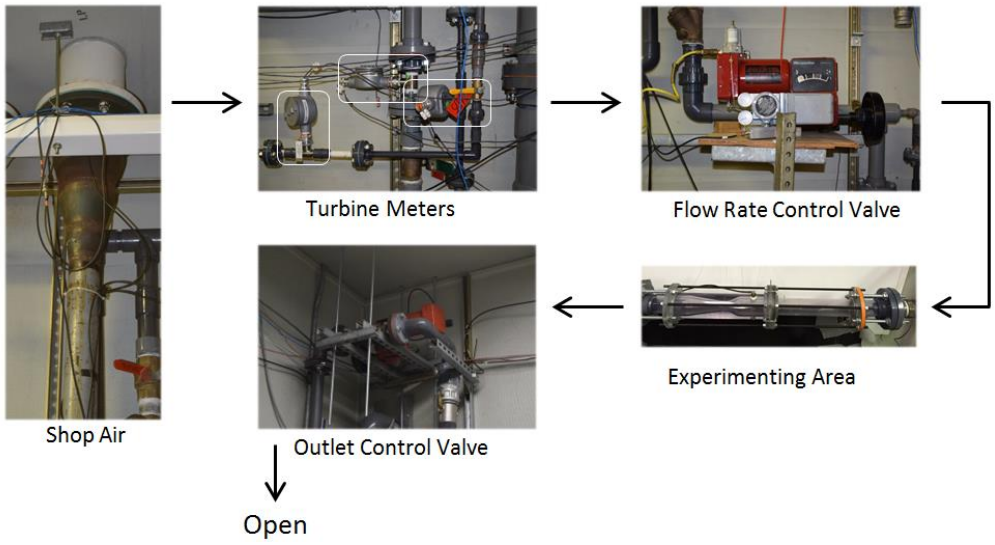


Figure 4.3 Flow diagram of air supply system

4.1.3 Experiment System

Water and air are mixed and enter the experiment system which can be divided into three main parts, the upstream pipe, slotted orifice with holding flanges, and Venturi

pipe. The upstream a transparent schedule 80 PVC pipe with inner diameter of the 2 inches and length of 5 times its inner diameter, the length required for the slotted orifice plate to perform accurately. The slotted orifice plate that is used in this experiment has a beta ratio of 0.467 and is 0.25 inches thickness. Two non-standard Polycarbonate flanges hold the slotted orifice plate in place and aligned. The Venturi pipe is also made of Polycarbonate with 3-D printing. The entrance and throat diameters are 1.9048 and 0.9075 inches respectively, and the length of the Venturi pipe is 13 inches. Pressures are measured using four PX429-150GI pressure transducers at 1 inch upstream and downstream of the slotted orifice plate and the entrance, and throat of the Venturi pipe, and one PX429-250GV pressure transducer at the diffuser part of the Venturi pipe. All five pressure transducers output 4-20 mA current within their working range. Specifications of pressure transdusers are listed in Table 4.3.

Table 4.3 Specifications of pressure transducers

| Amount | Manufacturer | Model | Range (psi) | Uncertainty |
|---|---|---|---|---|
| 4 | Omega Engineering | PX429-150GI | 0-150 | 0.275% |
| 1 | Omega Engineering | PX429-250GI | 0-250 | 0.275% |

Two impedance electrodes made of ultra-machinable brass are place on the Venturi at two inches from the slotted orifice plate. Temperature of the flow is also measured with an Omege T-Type thermocouple 5 inches from the Venturi pipe, and the measuring uncertainty of the thermocouple is below 0.5%. Figure 4.4 displays a schematic

diagram of the experimenting section, and Figure 4.5, Figure 4.6 are the actual photos of the assembly of the experimenting section, the slotted orifice plate and one of the electrodes.

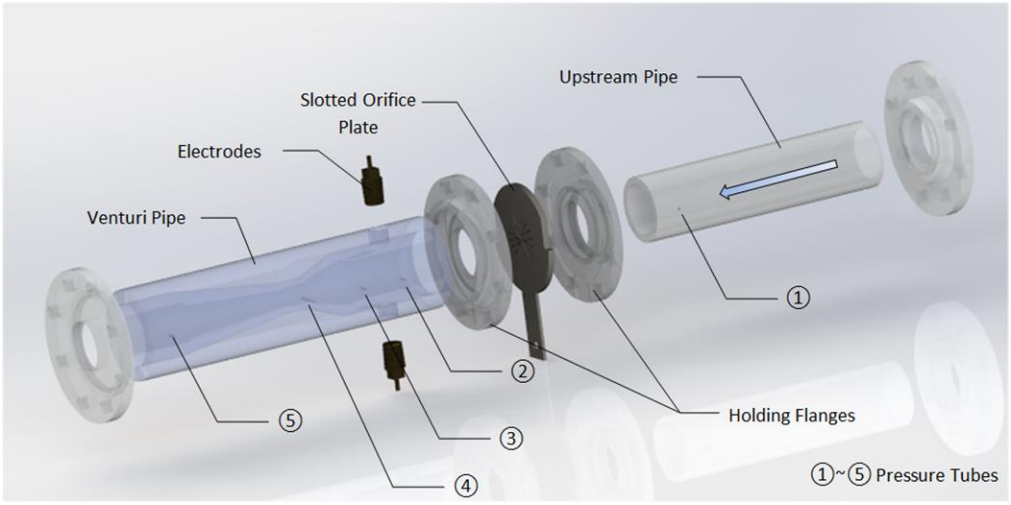


Figure 4.4 Schematic diagram of experimenting section

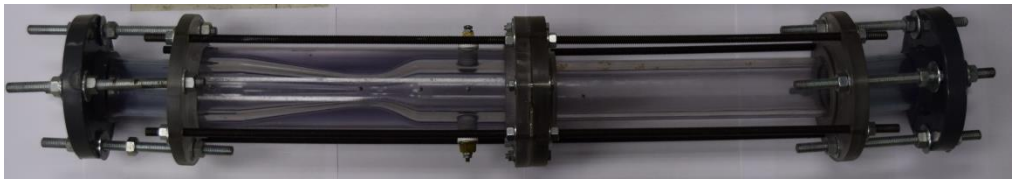

Figure 4.5 Actual assembly of experimenting section

Figure 4.6 Slotted orifice and electrode

Two electrodes are connected to an experimental circuit. The circuit uses Texas Instrument LM-7171 op-amp configuration showed in Figure 4.7 and is supplied with DC at 15 V.

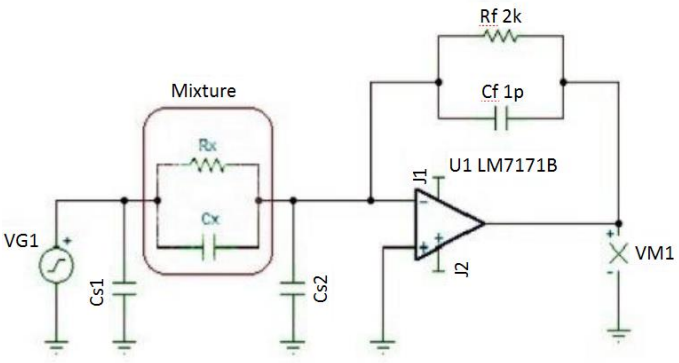


Figure 4.7 Op-amp configuration

A Picoscope-5252 that has two input channels and one output channel is used to generate signals and receive responding signals. Three signals are sent to the computer where they are analyzed and stored by a LabView program.

### 4.1.4 Visualization System

The principle of visualization study of this study to record videos for the flows being homogenized by the slotted orifice plate with a high speed camera since the Veturi pipe is transparent.

A 4 ft. by 2 ft. dimmable LED panel that can provide 6600 Lumens of 5000 K cool white color light is installed on the back wall of the experimenting section, since high speed videos require more light input than other ordinary videos. In order to improve video quality and get better contrast of the flow against the ambient, the LED panel is cover with two black painted boards with a 3.5 inches gap in between.

During experiments, videos are taken with a Phantom V711 high speed camera showed in Figure 4.8. Video taking specifications are listed in the table below.

Table 4.4 Specifications of high speed videos

| Resolution | Sample Rate | Exposure Time |
|---|---|---|
| 1280 x 720 | 1000 fps | 249.647 $\mu$s |

A Sony Handycam HDR-CX560V Camcorder is also set up to take 60 fps videos for 6s time length for the purpose of recording and analyzing flow patterns.


Figure 4.8 Phantom V711 high speed camera

## 4.2 Experimental Methods

### 4.2.1 Measurement Procedure

The data taking process started in December 2015 after a few months of making non-standard parts and setting up the experimental equipment. Measurements and videos were taken with the experimental section placed horizontally and vertically facing downward. Operation range of measurement is:

– Water flow rate (GPM): 10, 20, 30, 40, 50, 60, 70, 80

– Pressure (PSI): 20, 40, 60

– Gas Volume Fraction (%):2.5, 5, 7.5, 10, 20, 30, 40, 50, 60, 70, 80, 90, 95, 97.5

– Temperature (°F): 80-100

For the experimenting process, a LabView program is used to control water and air flow rate, pressure, and GVF of the flow and to display as well as record measured

results from pressure transducers, thermocouples, and flow meters. At the same time, all electrical signals emitted and received by the electrodes are monitored and recorded by another LabView program. The interfaces of the LabView program are shown in Figure 4.9 and Figure 4.10.


Figure 4.9 LabView interface for measurement and control

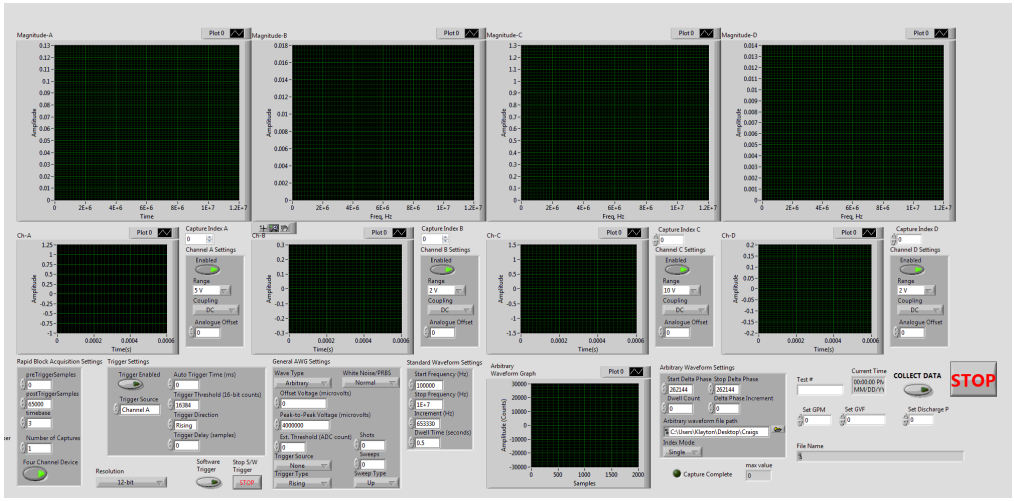


Figure 4.10 LabView interface for signal processing

### 4.2.2 Data Acquisition

The impedance measurement uses twelve sinusoidal signals with the same amplitudes but various frequencies. Their frequencies are 200 kHz, 600 kHz, 1 MHz, 1.28 MHz, 2.37 MHz, 3.46 MHz, 4.55 MHz, 5.64 MHz, 6.73 MHz, 7.82 MHz, 8.91 MHz, and 10 MHz respectively. During the experiment, all response signals are acquired via the input channel of the Data Acquisition (DAQ) system. Amplitude gains and phase changes are calculated by comparing the excitation and response signals for every frequency. Finally, all the data is saved in .csv format which can be opened and manipulated with Microsoft Excel.

### 4.2.3 Data Processing and Calculation

Relationships between the impedance of mixed flows and GVFs are determined by plotting measured amplitude gains and phases changes versus GVFs measured by turbine meters for a series of signal frequencies. GVF can be determined with water and air volumetric flow rates measured with conventional turbine meters

$$GVF = \frac{\dot{Q}_{air}}{\dot{Q}_{water} + \dot{Q}_{air}} \tag{4.1}$$

Air density is crucial to calculate the bulk volumetric flow rate of the mixture in the next step. Density of air can be calculated using the Ideal Gas Law using the local temperature and pressure under the ideal gas assumption.

$$\rho_{air} = \frac{P}{RT} \tag{4.2}$$

Because pressure changes as the mixture flows along the Venturi pipe, air density does not remain constant and consequently GVF changes. However, mass of both air and water remain constant all the time. So the mass based quality *X* is used to calculate the mixed density of air and water.

$$\begin{aligned} X &= \frac{\dot{m}_{air}}{\dot{m}_{air} + \dot{m}_{water}} \\ &= \frac{\dot{Q}_{air} \times \rho_{air}}{\dot{Q}_{air} \times \rho_{air} + \dot{Q}_{water} \times \rho_{water}} \\ &= \frac{\rho_{air}}{\rho_{air} + \frac{\dot{Q}_{water}}{\dot{Q}_{air}} \times \rho_{water}} \\ &= \frac{\rho_{air}}{\rho_{air} + \left(\frac{\dot{Q}_{water} + \dot{Q}_{air}}{\dot{Q}_{air}} - \frac{\dot{Q}_{air}}{\dot{Q}_{air}}\right) \times \rho_{water}} \\ &= \frac{\rho_{air}}{\rho_{air} + (\frac{1}{GVF} - 1) \times \rho_{water}} \end{aligned} \tag{4.3}$$

Using the quality of air, the density of the air-water mixture is calculated as

$$\rho_{mix} = \frac{\rho_{air}}{X + (1 - X)\rho_{air} / \rho_{water}} \tag{4.4}$$

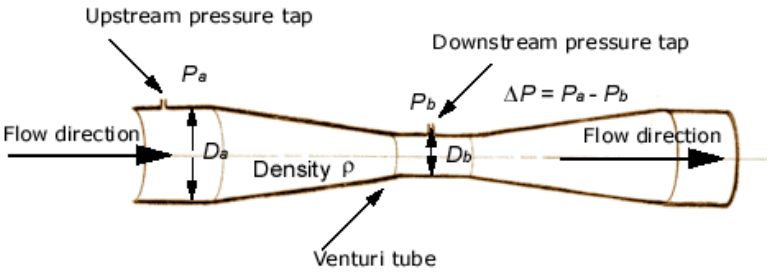


Figure 4.11 Venturi meter [37]

Bernoulli's equation is the basis to meter flow rate with a Venturi pipe. Figure 4.11 is a typical Venturi pipe.

$$\frac{1}{2}\rho_a v_a^2 + \rho_a g z_a + P_a = \frac{1}{2}\rho_b v_b^2 + \rho_b g z_b + P_b \tag{4.5}$$

Due to mass conservation of air,

$$\dot{Q}_{air,a}\rho_{air,a} = \dot{Q}_{air,b}\rho_{air,b} \tag{4.6}$$

$$\begin{aligned} \dot{Q}_{air,a} &= \frac{\rho_{air,b}}{\rho_{air,a}}\dot{Q}_{air,b} \\ &= \frac{P_a}{P_b}\frac{R}{R}\frac{T_a}{T_b}\,\dot{Q}_{air,b} \end{aligned} \tag{4.7}$$

For the process of air expansion from the high pressure at the inlet part to the low pressure at the throat part of the Venturi part, it is reasonable to be assumed isothermal, $T_a = T_b$.

$$\begin{aligned} \dot{Q}_{air,a} &= \frac{P_a}{P_b}\dot{Q}_{air,b} \\ \frac{P_b}{P_a}\dot{Q}_{air,a} &= \dot{Q}_{air,b} \end{aligned} \tag{4.8}$$

Unlike air, water is assumed to be incompressible and the density of it does not change. So the mass conservation of the mixture can be expressed as below.

$$\dot{Q}_{mix,a}\rho_{mix,a} = \dot{Q}_{mix,b}\rho_{mix,b} \tag{4.9}$$

$$(\dot{Q}_{air,a} + \dot{Q}_{water})\rho_{mix,a} = \left(\dot{Q}_{air,b} + \dot{Q}_{water}\right)\rho_{mix,b} \tag{4.10}$$

$$\left(\dot{Q}_{air,b} + \dot{Q}_{water}\right) = \frac{\rho_{mix,a}}{\rho_{mix,b}}\left(\dot{Q}_{air,a} + \dot{Q}_{water}\right) \tag{4.11}$$

Since for the mixture, volumetric flow rate is equal to velocity times the cross-sectional area of the pipe, $\dot{Q}_{mix} = v_{mix}A$, velocities of the mixture are expressed as

$$v_{mix,a} = \frac{\dot{Q}_{air,a} + \dot{Q}_{water}}{A_a} \tag{4.12}$$

$$\begin{aligned} v_{mix,b} &= \frac{\dot{Q}_{air,b} + \dot{Q}_{water}}{A_b} \\ &= \frac{\left(\frac{P_b}{P_a}\dot{Q}_{air,a} + \dot{Q}_{water}\right)\frac{\rho_{mix,a}}{\rho_{mix,b}}}{A_b} \\ &= \frac{\left(\frac{P_b}{P_a}\cdot GVF_a + (1 - GVF_a)\right)\dot{Q}_{mix,a}\frac{\rho_{mix,a}}{\rho_{mix,b}}}{A_b} \\ &= \frac{\left(\frac{P_b}{P_a}\cdot GVF_a + (1 - GVF_a)\right)\frac{\rho_{mix,a}}{\rho_{mix,b}}\,A_a}{A_b}v_{mix,a} \\ &= \left(\frac{P_b}{P_a}\cdot GVF_a + (1 - GVF_a)\right)\frac{\rho_{mix,a}}{\rho_{mix,b}}\beta^2 v_{mix,a} \\ &= \lambda\beta^2 v_{mix,a} \end{aligned} \tag{4.13}$$

$$\lambda = \left(\frac{P_b}{P_a} \cdot GVF_a + (1 - GVF_a)\right)\frac{\rho_{mix,a}}{\rho_{mix,b}} \tag{4.14}$$

Where $\beta$ is the ratio of the diameter of the throat to the diameter of the inlet of the Venturi pipe, $\beta = \frac{D_a}{D_b}$.

With the relationship between $v_{mix,a}$ and $v_{mix,b}$ that derived in equation (4.12), volumetric flow rate and mass flow rate of the mixture at the inlet part of the Venturi pipe can be calculated. When the Venturi pipe is placed vertically, the gravitational terms $\rho_a g z_a$ and $\rho_b g z_b$ are hard to calculate because the densities at both points are not the same and there is a height variation. In this case, the arithmetic mean value of the two densities is used to simplify the calculation such that the difference of the two terms becomes

$$\rho_a g z_a - \rho_b g z_b \approx \rho_{ave} g h \tag{4.15}$$

$$\rho_{ave} = \frac{1}{2}(\rho_a + \rho_b) \tag{4.16}$$

$$h = z_a - z_b \tag{4.17}$$

Equations are stated blow for both horizontal and vertical setups.

Horizontal

$$\dot{Q}_{mix,a} = C_{d,v}\sqrt{\frac{2(P_a - P_b)}{\lambda^2 \beta^4 \rho_b - \rho_a}} \cdot \frac{1}{4}\pi D_a^2 \tag{4.18}$$

$$\dot{M}_{mix,a} = \dot{Q}_{mix,a}\rho_{mix,a} \tag{4.19}$$

Vertical

$$\dot{Q}_{mix,a} = C_{d,v}\sqrt{\frac{2(P_a - P_b + \rho_{ave}gh)}{\lambda^2\beta^4\rho_b - \rho_a}} \cdot \frac{1}{4}\pi D_a^2 \tag{4.20}$$

$$\dot{M}_{mix,a} = \dot{Q}_{mix,a}\rho_{mix,a} \tag{4.21}$$

where $C_{d,V}$ is the discharge coefficient of the Venturi pipe.

At last, discharge coefficient of the slotted orifice plate $C_{d,p}$ can be calculated using the standard equation for slotted orifice plate meters

$$C_{d,p} = \frac{\dot{m}\sqrt{1-\alpha^4}}{A_f\sqrt{2\rho\Delta P}} \tag{4.22}$$

where $\dot{m}$ is the total mass flow rate of the mixture, $\alpha$ is the area ratio of the slotted orifice plate which is 0.467 in this study, $A_f$ is the flow area of the slotted orifice plate meter, $\rho$ is the mass based density of the mixture under downstream condition and $\Delta P$ is the pressure drop across the plate.

### 4.2.4 Visualization Analysis

Visualization analysis is conducted in this study to study the homogenization ability of the slotted orifice plate. High speed videos of the flow passing through the slotted orifice plate are taken with a high speed camera with a rate of 1000 frames per second

(fps), and saved in .cine and .avi formats for further analysis with MatLab software. In MatLab, each video is converted to gray level pictures frame by frame with 0 being black and 255 being pure white. The standard deviation of gray level of every pixel represents the homogenized level of the flow in this region. During analysis, four analyzing zones are chosen, the width of which are equal to the diameter of the electrodes and the heights are the diameter of the flow. The four zones are located at 1 inch upstream, 2, 2.5, and 3 inches downstream from the slotted orifice plate, in order to first compare the homogenized level of the flow before and after the plate, and second determine the best place where the flow is the most homogenized and steady.

# 5 RESULTS AND DISCUSSIONS

## 5.1 Tested Flow Conditions

Due to some limitations of the testing facilities, some flow conditions could not be tested. Table 5.1, Table 5.2 and Table 5.3 show all the flow conditions that were tested.

– The smallest air flow rate that the turbine flow meter can measure was 0.35 ACFM, thus low GVF with low water flow rate flow conditions were not practical

– The air supply was at a pressure of 110 PSI, so high GVF with low discharge pressure flow conditions were not able to be reached.

– The water supply was at a pressure of 120 PSI, so it could not provide sufficient water if high water flow rate and high discharge pressure were both desired.

display all flow conditions that were tested.

Table 5.1 Tested flow conditions at 20 PSI

| 20 PSI | | | | | | | | |
|---|---|---|---|---|---|---|---|---|
| GPM / GVF(%) | 10 | 20 | 30 | 40 | 50 | 60 | 70 | 80 |
| 0 | | | | | | | | |
| 2.5 | | | | | | | | |
| 5 | | | | | | | | |
| 7.5 | | | | | | | | |
| 10 | | | | √ | | | | |
| 20 | | √ | √ | √ | | | | |
| 30 | | √ | √ | √ | | | | |
| 40 | | √ | √ | | | | | |
| 50 | √ | √ | √ | | | | | |
| 60 | √ | √ | √ | | | | | |
| 70 | √ | √ | | | | | | |
| 80 | √ | √ | | | | | | |
| 90 | √ | √ | | | | | | |

Table 5.1 Continued

| | | | | | | | | |
|---|---|---|---|---|---|---|---|---|
| 95 | | | | | | | | |
| 97.5 | | | | | | | | |

Table 5.2 Tested flow conditions at 40 PSI

40 PSI

| GPM / GVF(%) | 10 | 20 | 30 | 40 | 50 | 60 | 70 | 80 |
|---|---|---|---|---|---|---|---|---|
| 0 | | | | | | | | |
| 2.5 | | | | | | | | |
| 5 | | | | | | | | |
| 7.5 | | | | | | | | |
| 10 | | | | √ | √ | √ | | |
| 20 | | √ | √ | √ | √ | √ | | |
| 30 | | √ | √ | √ | √ | | | |
| 40 | | √ | √ | √ | √ | | | |
| 50 | √ | √ | √ | √ | | | | |
| 60 | √ | √ | √ | √ | | | | |
| 70 | √ | √ | √ | √ | | | | |
| 80 | √ | √ | √ | | | | | |
| 90 | √ | √ | | | | | | |
| 95 | √ | | | | | | | |
| 97.5 | √ | | | | | | | |

Table 5.3 Tested flow conditions at 60 PSI

60 PSI

| GPM / GVF(%) | 10 | 20 | 30 | 40 | 50 | 60 | 70 | 80 |
|---|---|---|---|---|---|---|---|---|
| 0 | √ | √ | √ | √ | √ | √ | √ | √ |
| 2.5 | | | | | | √ | √ | √ |
| 5 | | | | | √ | √ | √ | √ |
| 7.5 | | | | | √ | √ | √ | √ |
| 10 | | | | √ | √ | √ | √ | √ |
| 20 | | | √ | √ | √ | √ | √ | |
| 30 | | | √ | √ | √ | √ | √ | |
| 40 | √ | √ | √ | √ | √ | √ | | |
| 50 | √ | √ | √ | √ | √ | √ | | |

Table 5.3 Continued

| | | | | | | | | |
|---|---|---|---|---|---|---|---|---|
| 60 | √ | √ | √ | √ | √ | √ | | |
| 70 | √ | √ | √ | √ | √ | | | |
| 80 | √ | √ | √ | √ | | | | |
| 90 | √ | √ | √ | | | | | |
| 95 | √ | √ | | | | | | |
| 97.5 | √ | | | | | | | |

## 5.2 GVF Measurement

For every flow condition and frequency, the signal gain $G$is calculated by dividing the output signal amplitude by the amplitude of the input signal that is generated by the Picoscope.

$$Gain = \frac{Output\ Signal\ Amplitude}{Input\ Signal\ Amplitude} \tag{5.1}$$

As plotted in Table 5.4, a trend can be observed that the gain decreases as the GVF increases for all frequencies. When it comes to phase angle displayed in Table 5.5, it shows a trend to decrease as the GVF increases for high frequencies, but for lower frequencies, there is not visible trend.

Table 5.4 Signal gain vs. GVF for all frequencies

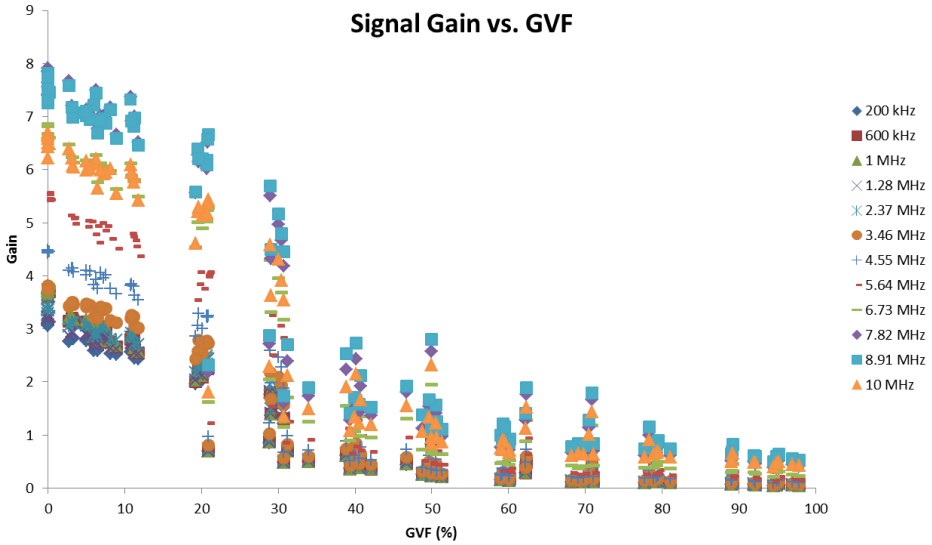


Table 5.5 Phase angle vs. GVF for all frequencies

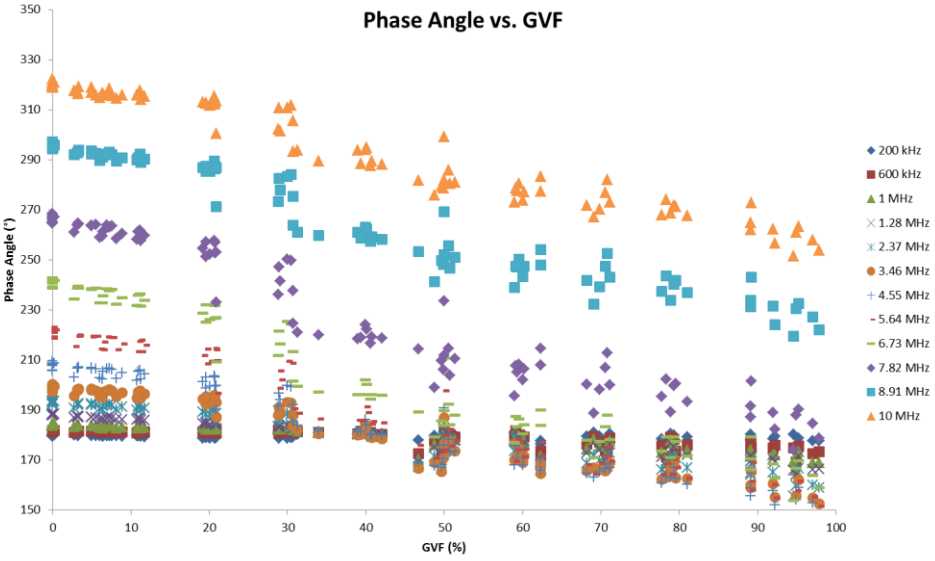


Sihombing's study showed that temperature had a linear effect on the signal gains [36], so it is possible to derive an equation about the impedance gain as a function of

temperature and GVF. Table 5.6 is a plot of the gain versus temperature at constant flow rate, pressure and GVF.

Table 5.6 Signal gain vs. temperature for all frequencies at 50 GPM 10 PSI 0 GVF

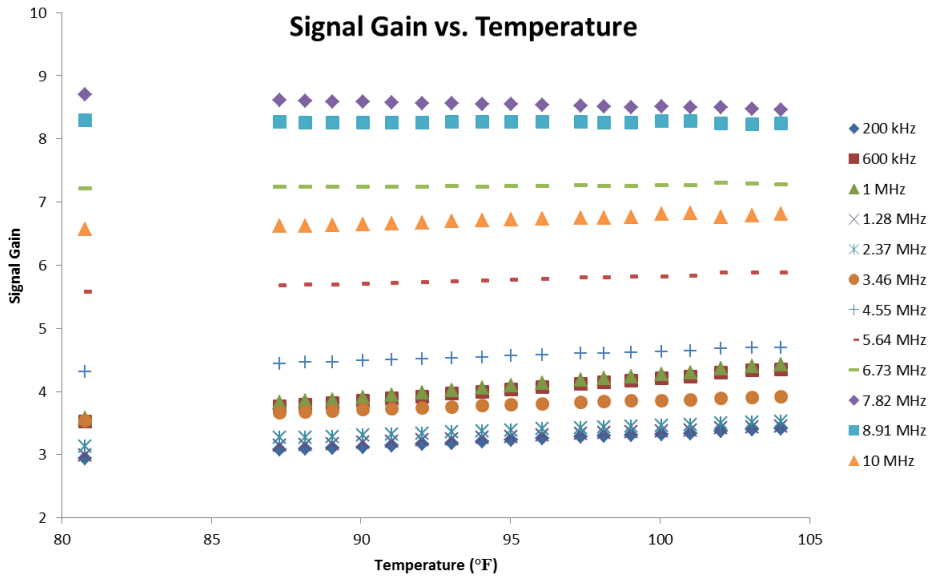


Then linear regressions can be applied to the data in order to calculate the factor to modify the signal gains to be at the effectively same temperature. Coefficients of the regressions for signals at all frequencies are listed in Table 5.7.

Table 5.7 Linear regressions for signal gain at 50 GPM 10 PSI 0 GVF

| $Gain = aT + b$ | | |
|---|---|---|
| Frequency | $a$ | $b$ |
| 200 kHz | 0.0201 | 1.3141 |
| 600 kHz | 0.0357 | 0.6420 |
| 1 MHz | 0.0366 | 0.6203 |

Table 5.7 Continued

| | | |
|---|---|---|
| 1.28 MHz | 0.0192 | 1.4615 |
| 2.37 MHz | 0.0166 | 1.8117 |
| 3.46 MHz | 0.0157 | 2.2918 |
| 4.55 MHz | 0.0157 | 3.0684 |
| 5.64 MHz | 0.0130 | 4.5378 |
| 6.73 MHz | 0.0027 | 6.9964 |
| 7.82 MHz | -0.0089 | 9.3924 |
| 8.91 MHz | -0.0014 | 8.3939 |
| 10 MHz | 0.0114 | 5.6356 |

A linear relationship is also found between phase angle and temperature in Table 5.8. And coefficients of the regressions for signals at all frequencies are listed in Table 5.9

Table 5.8 Phase angle vs. temperature for all frequencies at 50 GPM 10 PSI 0 GVF

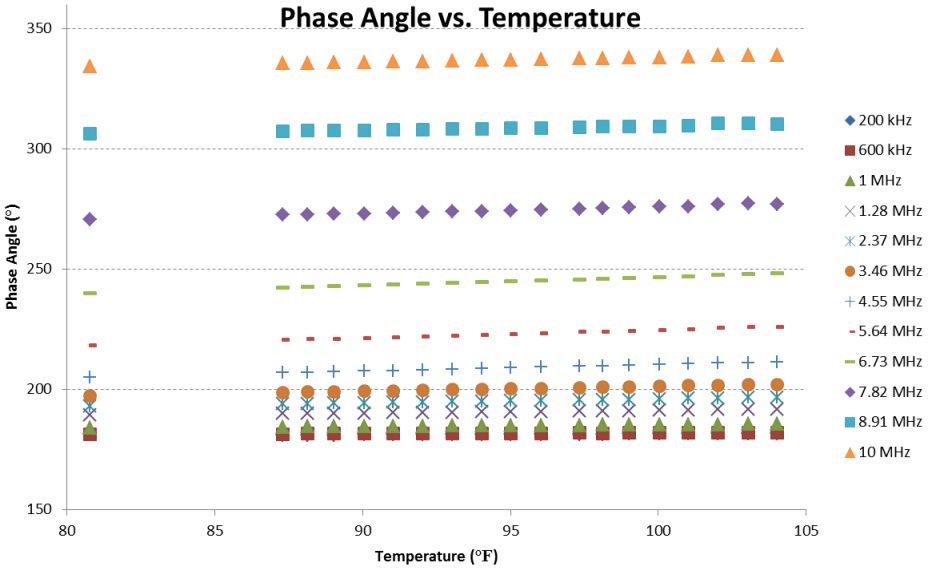

Table 5.9 Linear regressions for phase angle at 50 GPM 10 PSI 0 GVF

| $Phase\ angle = cT + d$ | | |
|---|---|---|
| Frequency | $c$ | $d$ |
| 200 kHz | 0.0310 | 178.48 |
| 600 kHz | 0.0271 | 179.18 |
| 1 MHz | 0.0652 | 178.80 |
| 1.28 MHz | 0.1077 | 180.46 |
| 2.37 MHz | 0.1616 | 179.88 |
| 3.46 MHz | 0.2081 | 180.52 |
| 4.55 MHz | 0.2685 | 183.31 |
| 5.64 MHz | 0.3336 | 191.36 |
| 6.73 MHz | 0.3554 | 211.19 |
| 7.82 MHz | 0.2864 | 247.29 |
| 8.91 MHz | 0.1900 | 290.57 |
| 10 MHz | 0.2049 | 317.55 |

The signal at 1 MHz frequency is chosen to analyze the signal gain and phase angle, because according to Sihombing's study, the most accurate result was yielded using the 1 MHz frequency, and he also introduced a function to eliminate the effect of temperature.

Table 5.10 Surface fitting of GVF vs. Gain and Temperature at 1 MHz

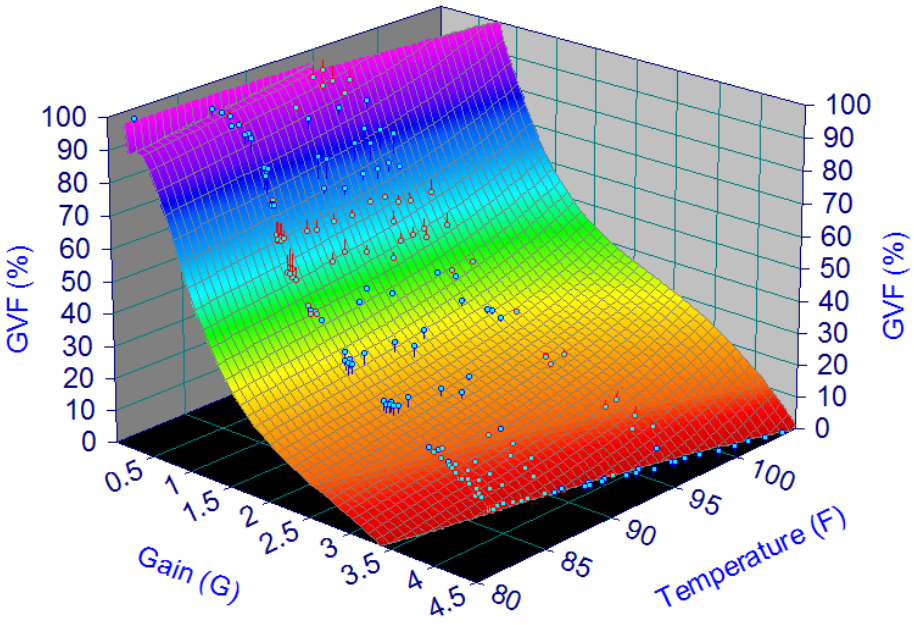


Table 5.10 is a 3-D plot of GVF as a function of signal gain and temperature. As can be seen in the figure, temperature has a significant effect on GVF, especially when GVF is below 30%.

A modified gain ($G'$) is introduced with the purpose to eliminate the effect of temperature. [37]

$$G' = \frac{G}{0.002T^{1.3}} \qquad [37] \qquad (5.2)$$

With this process done, it can be observed in Table 5.11 that most of the temperature effect is eliminated and the modified gain ($G'$) can be considered independent from temperature.

Table 5.11 Surface fitting of GVF vs. Modified Gain and Temperature at 1 MHz

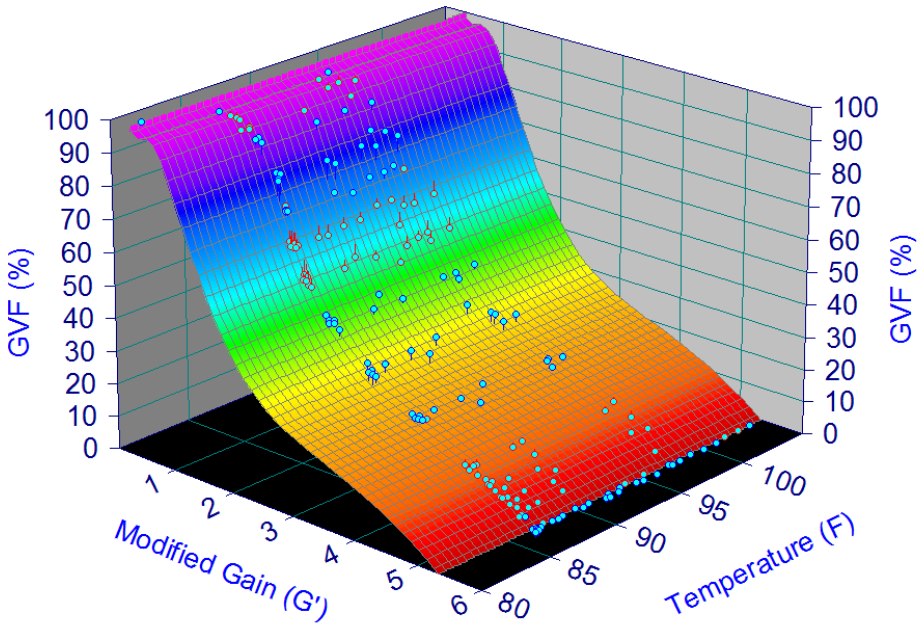


Since now the GVF is only a function of modified gain, a new plot is generated. Then the equation to calculate GVF from modified gain can be obtained by curve fitting with a $6^{th}$ order polynomial.

Table 5.12 Plot of GVF vs. G' with error bars

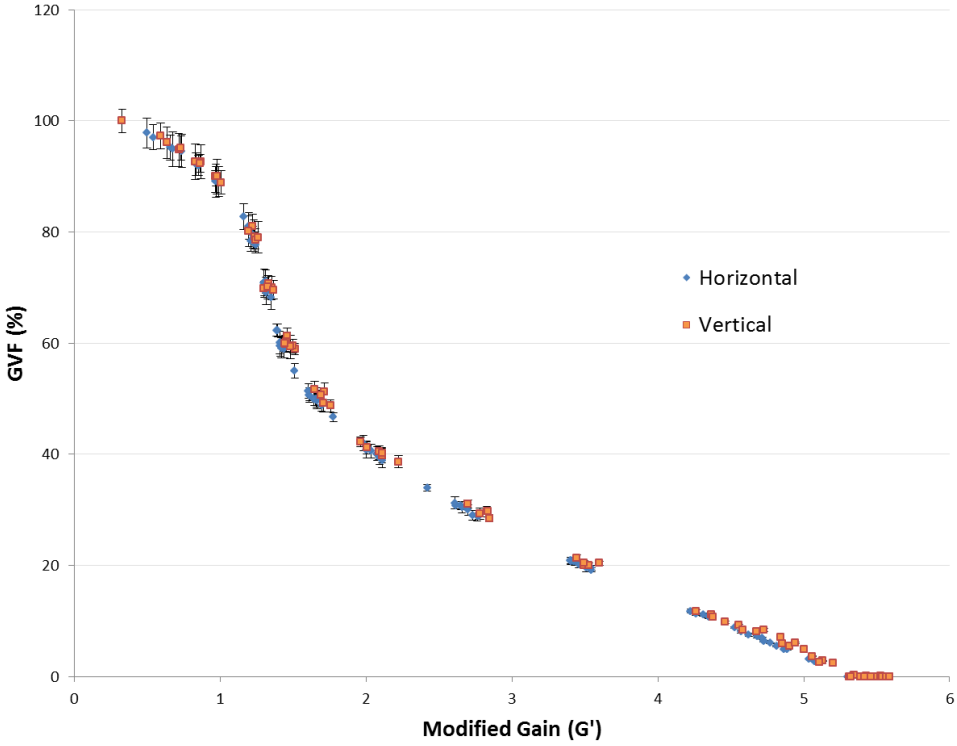


It can be observed in Table 5.12 that the two curves almost overlap each other, which means that the orientation of the test section has very little influence on the results of the signal gain measurement. With the consideration of accuracy, the equations are stated below separately.

Horizontal

$$\begin{aligned} GVF = \; & -0.4957\,G'^{6} + 9.3528\,G'^{5} - 69.203\,G'^{4} + 251.79\,G'^{3} \\ & -456\,G'^{2} + 337.54\,G' + 13.907 \\ R^2 = \; & 0.9954 \end{aligned} \tag{5.3}$$

Vertical

$$GVF = -0.2037\,G'^{6} + 4.2494\,G'^{5} - 34.858\,G'^{4} + 136.85\,G'^{3} - 262.53\,G'^{2} + 184.24\,G' + 58.75 \quad (5.4)$$

$$R^2 = 0.9954$$

With the above equations stated, a new plot of actual GVF vs. calculated GVF can be generated.

Table 5.13 Actual GVF vs. calculated GVF

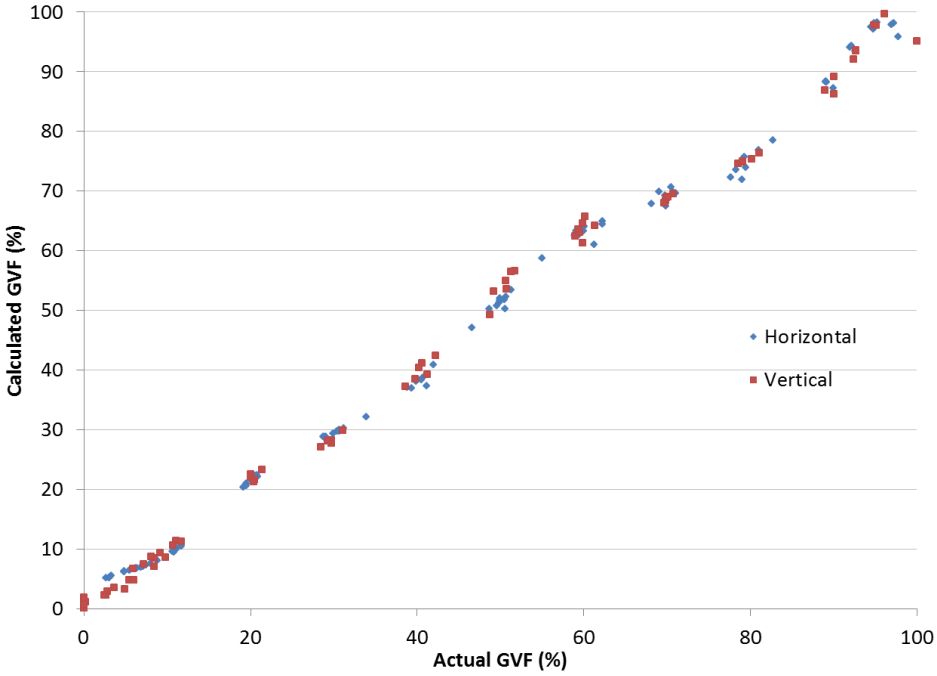

Table 5.13 shows that the calculated GVF has a linear correlation with the actual GVF. The uncertainties of the GVF measurements are ±3.523% in the horizontal orientation and ±4.320% in the vertical orientation, which are smaller than the ±5.5% uncertainty from Sihombing's results [37].

When it comes to the phase angle, it does not vary much as GVF increases for the 1 MHz signal as shown in Table 5.5. So the 10 MHz signal is chose for the phase angle analysis for the phase angle having large variation between low and high GVF values and low sensitivity to temperature as indicating in Table 5.9

Table 5.14 Plot of GVF vs. phase angle

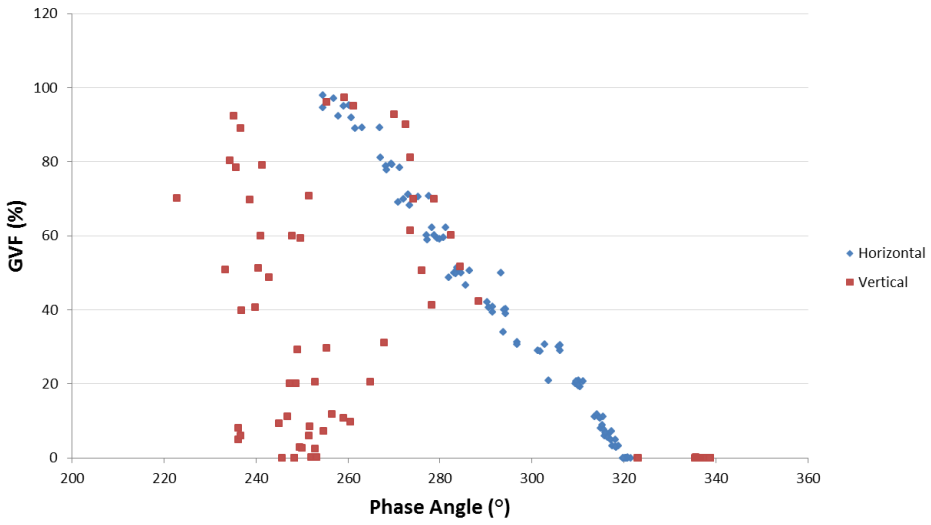

As displayed in Table 5.14, the GVF shows a good linear relationship with the phase angle only when the test section is in the horizontal orientation. The equation is stated below.

$$GVF = -1.4697\,\psi + 472.12$$
$$R^2 = 0.9861 \tag{5.5}$$

5.3 Flow Rate Measurement

Using equations 4.15-4.22 that stated in Data Processing part, the measured flow rates for all tested conditions are calculated and plotted versus the actual flow rates measured by turbine meters, where the Discharge Coefficient can be obtained by linear regression.

Table 5.15 Horizontal Venturi Result

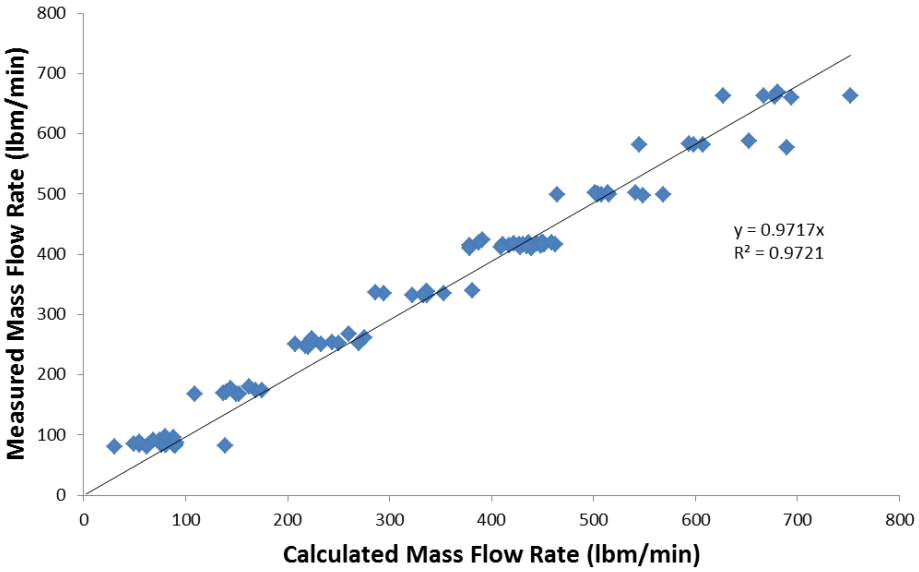


Table 5.16 Vertical Venturi Result

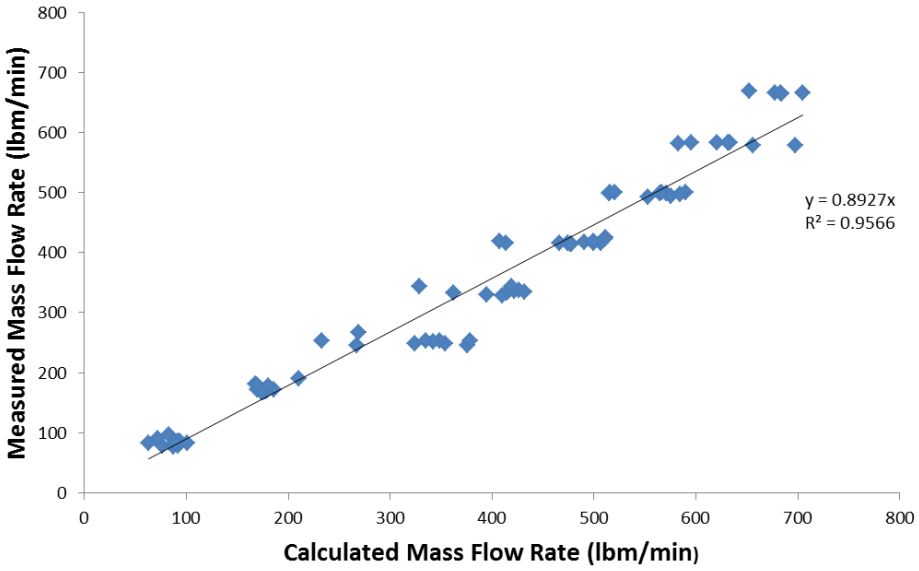

As shown in Table 5.15 and Table 5.16, the Discharge Coefficient of the Venturi pipe is 0.9717 when placed horizontally and 0.8927 when placed vertically. It is obvious that under the flow conditions that were tested, the Venturi pipe has higher discharge ability in horizontal orientation than in vertical orientation.

Table 5.17 Discharge Coefficient of the Slotted Orifice Plate placed horizontally

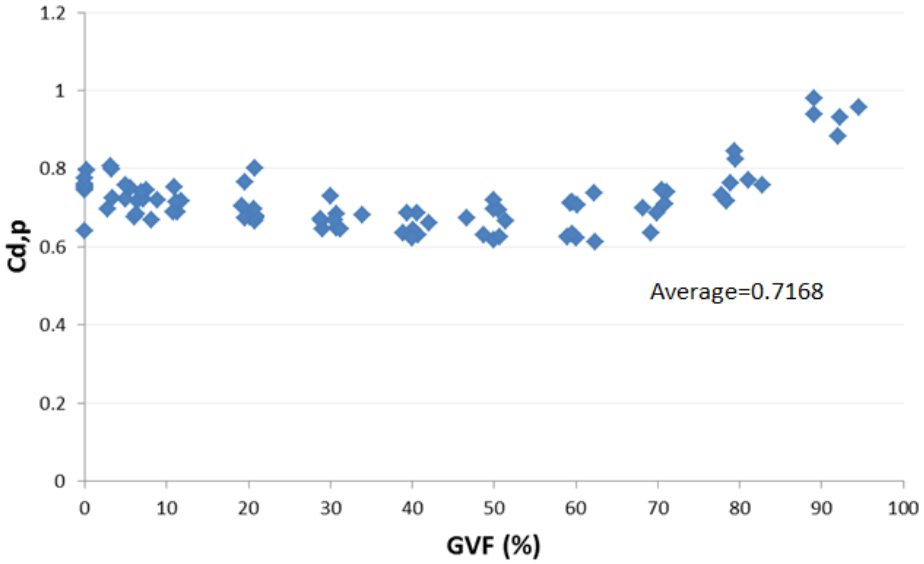

Table 5.18 Discharge Coefficient of the Slotted Orifice Plate placed vertically

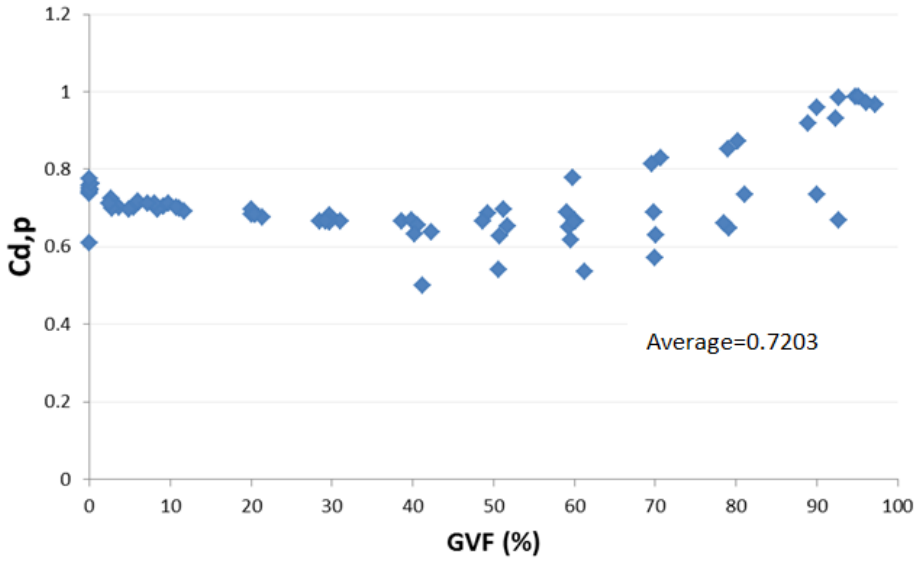


Table 5.17 and Table 5.18 display the calculated Discharge Coefficient of the Slotted Orifice Plate in both horizontal and vertical positions. It seems that orientation does not affect the discharge ability of the plate because the two average Discharge Coefficients are about equal. And in both tables, there appears a trend that the discharge ability of the Slotted Orifice Plate reaches its lowest point at medium GVF, and the Discharge Coefficient gets closed to 1 as the GVF increases to 100%.

## 5.4 Homogenize Ability of Slotted Orifice Plate

This section is going to present the result of the visualization study about the homogenization ability of the slotted orifice plate by categorizing the flow for horizontal

and vertical orientations. Some detailed results will be shown for the flows in all flow regimes that were observed during the experiment.

### 5.4.1 Horizontal Flows

#### 5.4.1.1 Bubbly flow

A bubbly flow exhibited in Figure 5.1 happens at 80 GPM, 60 PSI and 10 GVF. The three rectangles on the left are the zones for analysis which are located 2, 2.5 and 3 inches downstream of the slotted orifice plate. And the rectangle on the right is the only upstream zone for analysis at 2.5 inches from the plate since the flow pattern does not change much before the interaction with the slotted orifice plate.

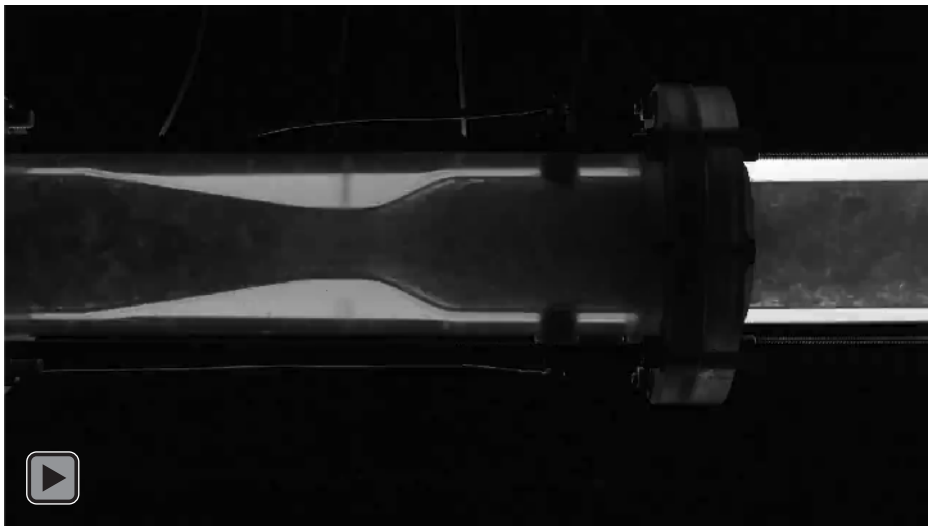

Video 5.1 Horizontal bubbly flow at 80 GPM 60 PSI 10 GVF

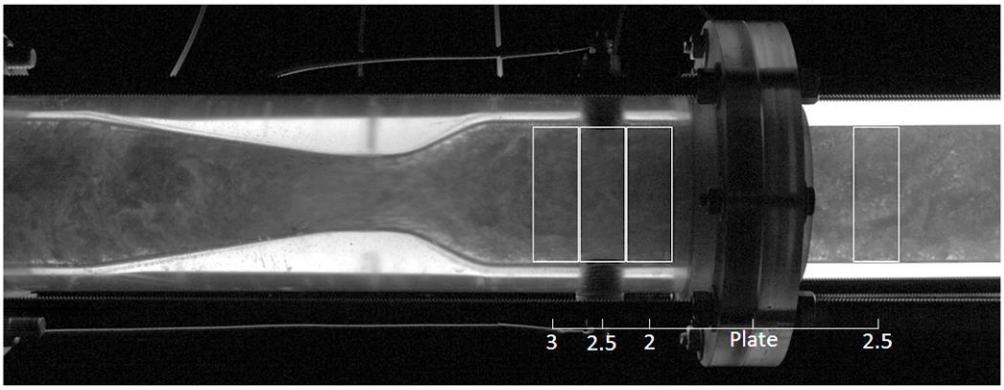

Figure 5.1 Horizontal bubbly flow at 80 GPM 60 PSI 10 GVF

As demonstrated in Figure 5.1, the width of an analysis zone is the same as the diameter of the electrodes and the height is equal to the inner diameter of the pipe. Intuitively, there are clear and recognizable black dots in the upstream flow which are air bubbles in the camera. On the contrary, there is only flocculent bubbles with no clear edges can be seen in the downstream flow after homogenized by the slotted orifice plate. To analyze the photos, the variation of standard deviation of gray level in each zone is calculated and plotted frame by frame generating a line chart.

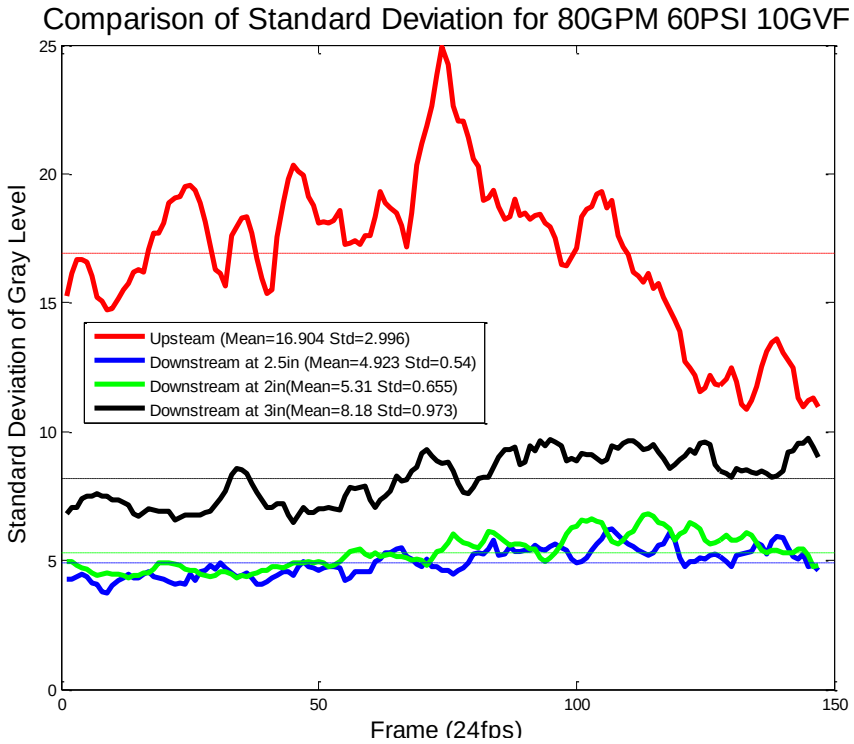


Figure 5.2 Comparison of homogenized level for horizontal bubbly flow

As indicated in Figure 5.2, the standard deviations of gray level in the downstream at all three locations are much less than the zone in the upstream, and all the actual values are listed in Table 5.19. The minimum mean value of standard deviation of gray level is no more than 1/3 of that of the upstream flow. Moreover, the standard deviation of all values in the downstream with respect to time is much less than in the upstream meaning that the flow has become more of a steady state after being homogenized by the slotted orifice plate. By comparing the results among the three downstream zones, flow at 2.5 inches from the plate seems to be the most homogenized and steady.

Table 5.19 Comparison of homogenized level for horizontal bubbly flow

| Zone | Mean | Standard Deviation |
|---|---|---|
| Upstream | 16.904 | 2.996 |
| Downstream 2 in | 5.310 | 0.655 |
| Downstream 2.5 in | 4.923 | 0.540 |
| Downstream 3 in | 8.180 | 0.973 |

5.4.1.2 Plug flow

Figure 5.3 shows plug flow at 40 GPM, 20PSI and 10 GVF. A continueous layer of water can be observed at upstream flow, bigger bubbles are formed and concentrate at the top part of the flow. After passing the slotted orifice plate, no continueous layer of water or bubble concentration can be seen.

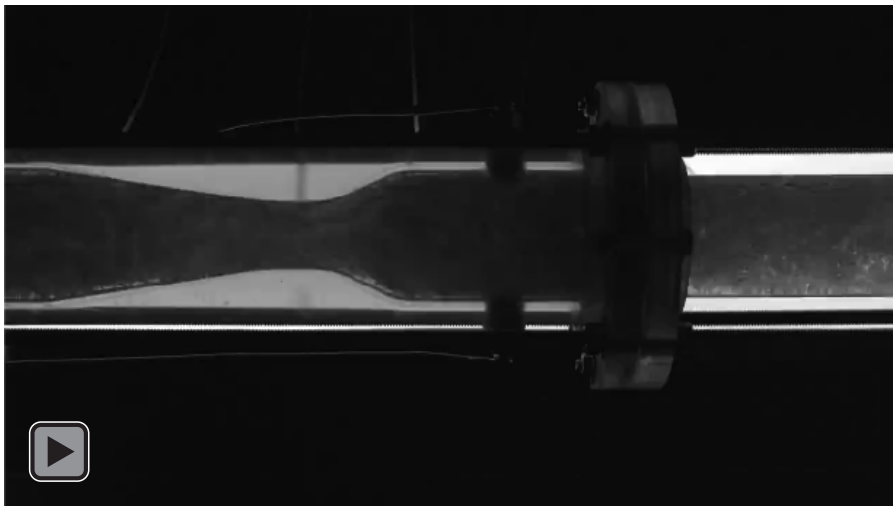

Video 5.2 Horizontal plug flow at 40 GPM 20 PSI 10 GVF

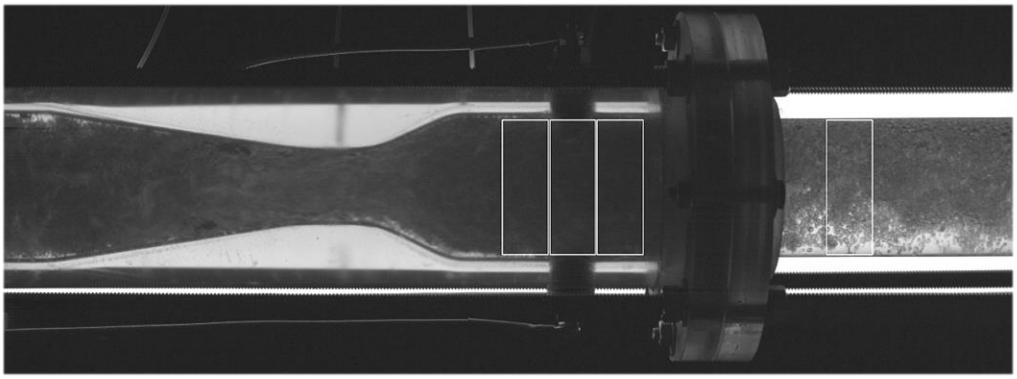

Figure 5.3 Horizontal plug flow at 40 GPM 20 PSI 10 GVF

Homogenize level is significantly improved with the help of slotted orifice plate. Mean value of standard deviation of gray level is reduced to approximately 1/10 of the initial value. Meanwhile, the well-mixed flow is much steadier than before. Figure 5.4 displays the change of homogenization level of the mixture intuitively, and Table 5.20 lists all the actual values.

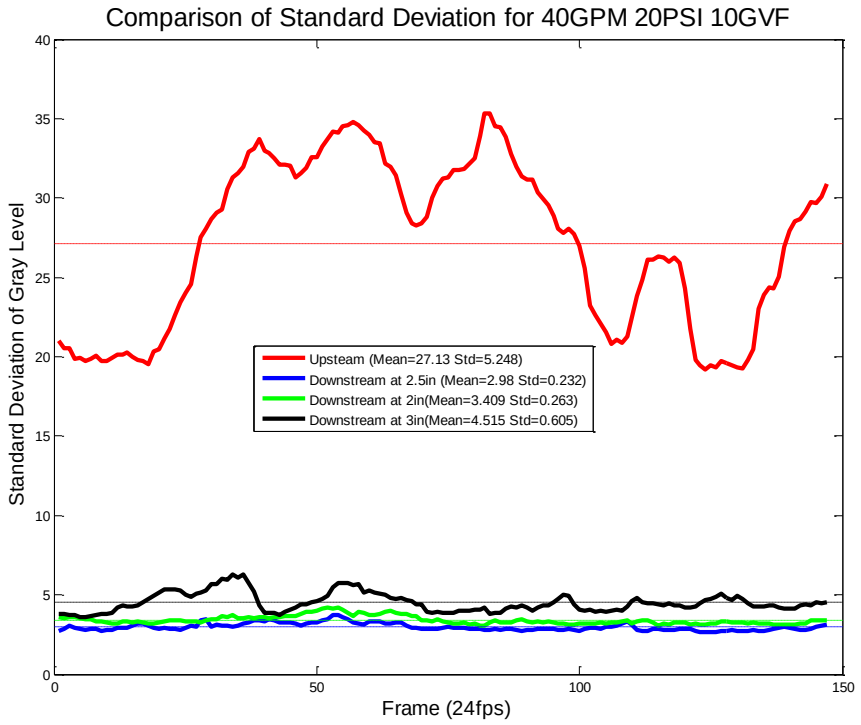


Figure 5.4 Comparison of homogenized level for horizontal plug flow

Table 5.20 Comparison of homogenized level for horizontal plug flow

| Zone | Mean | Standard Deviation |
|---|---|---|
| Upstream | 27.130 | 5.248 |
| Downstream 2 in | 3.409 | 0.263 |
| Downstream 2.5 in | 2.980 | 0.232 |
| Downstream 3 in | 4.515 | 0.605 |

5.4.1.3 Slug flow

Slug flow happens at 30 GPM, 40 PSI and 70 GVF is shown in Figure 5.5. Stratification and liquid slugs can be observed in the upstream flow, but neither can be seen in the downstream flow.

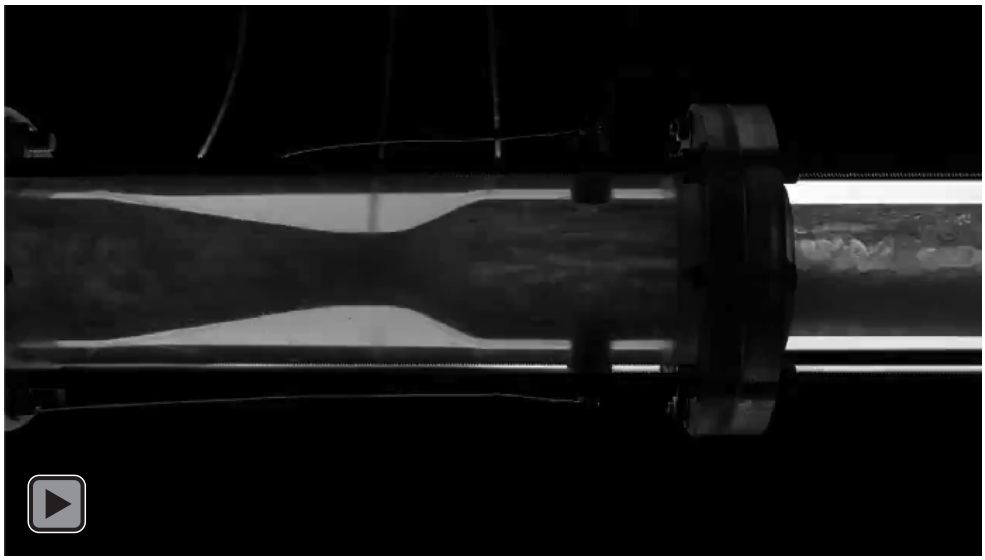

Video 5.3 Horizontal slug flow at 30 GPM 40 PSI 70 GVF

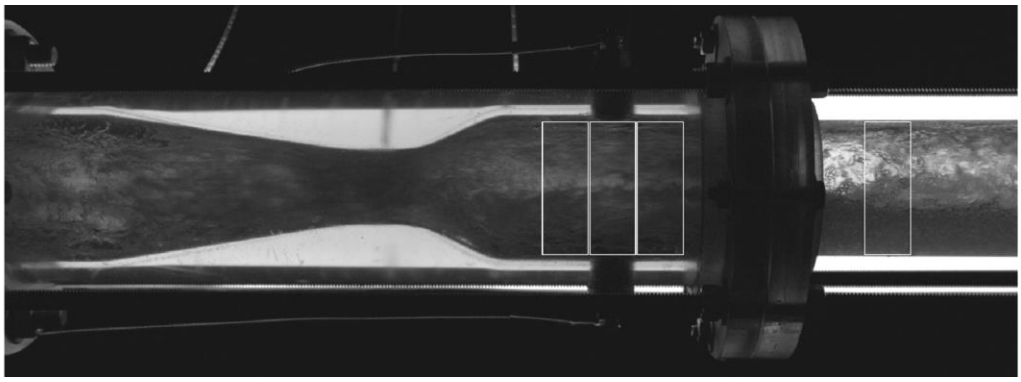

Figure 5.5 Horizontal slug flow at 30 GPM 40 PSI 70 GVF

As can be seen in Figure 5.6, both homogenized level and steady level are well improved yet mean values and standard deviations are still high comparing to bubbly flow and plug flow. A peak shows in the plot as a liquid slug passes through the analysis zones. The plots of downstream flows have similar shapes to that of the upstream flow but with

less amplitudes, which indicates the slotted orifice plate does have the ability to condition the flow, but still cannot eliminate the effects of liquid slugs completely. The downstream flow at 2 inches from the plate is more homogenized and steady than at 2.5 inches from the plate. Table 5.20 lists all the actual values of the results.

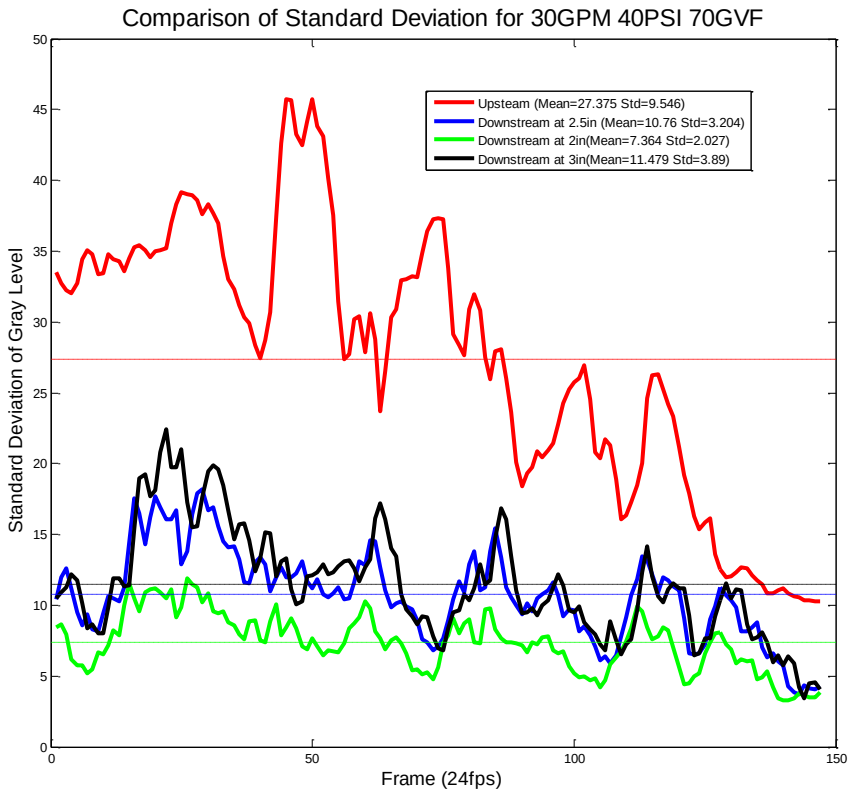


Figure 5.6 Comparison of homogenized level for horizontal slug flow

Table 5.21 Comparison of homogenized level for horizontal slug flow

| Zone | Mean | Standard Deviation |
|---|---|---|
| Upstream | 27.375 | 9.546 |
| Downstream 2 in | 7.364 | 2.027 |

Table 5.21 Continued

| | | |
|---|---|---|
| Downstream 2.5 in | 10.76 | 3.204 |
| Downstream 3 in | 11.479 | 3.89 |

5.4.1.4 Annular flow

Figure 5.7 demonstrates the annular flow happens at 20 GPM, 65 PSI and 95 GVF. Water is distributed well along the wall of the pipe in the upstream flow, and a core of air can be observed. Due to gravity, there is more water on the bottom of the pipe than on the top.

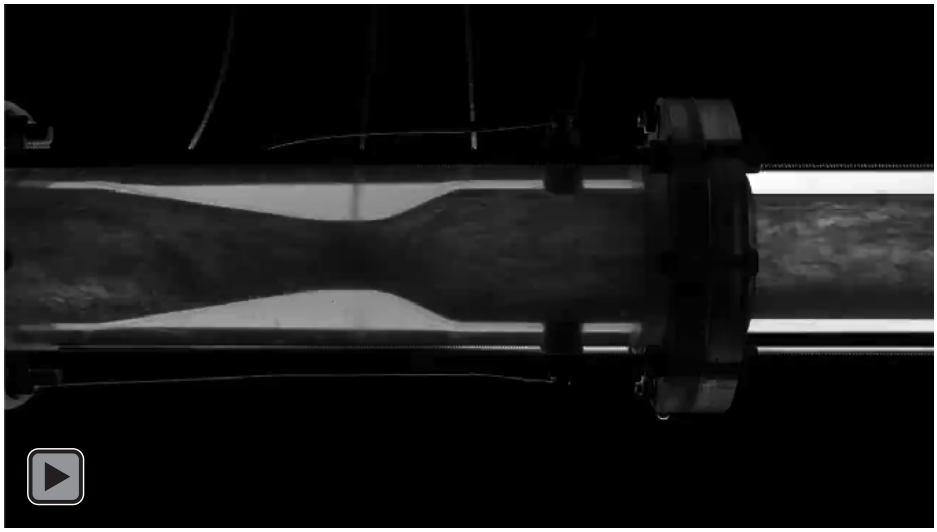

Video 5.4 Horizontal annular flow at 20 GPM 65 PSI 95 GVF

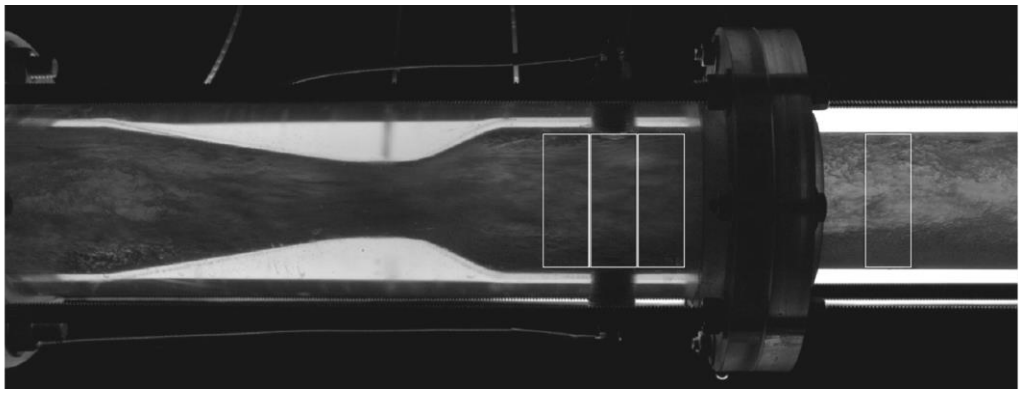

Figure 5.7 Horizontal annular flow at 20 GPM 65 PSI 95 GVF

As showed in Figure 5.8, the downstream flow is much more homogenized and steady comparing to the upstream flow. The most homogenized and steady place is 2 inches from the slotted orifice plate. All the actual values are listed in Table 5.22.

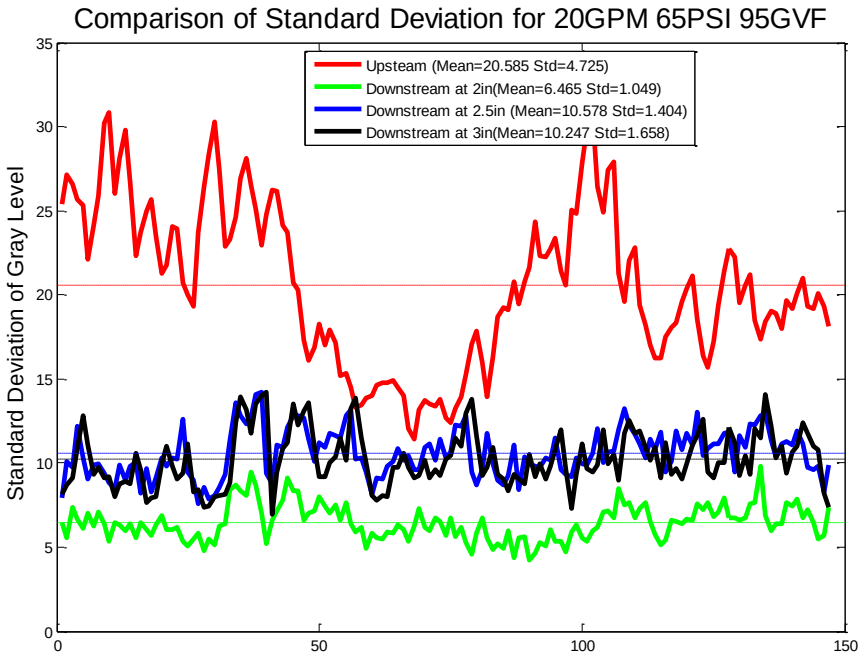


Figure 5.8 Comparison of homogenized level for horizontal annular flow

Table 5.22 Comparison of homogenized level for horizontal annular flow

| Zone | Mean | Standard Deviation |
|---|---|---|
| Upstream | 20.585 | 4.725 |
| Downstream 2 in | 6.465 | 1.049 |
| Downstream 2.5 in | 10.578 | 1.404 |
| Downstream 3 in | 10.247 | 1.658 |

### 5.4.2 Vertical Flows

#### 5.4.2.1 Bubbly flow

Figure 5.9 is a 90 degree rotated vertical bubbly flow happens at 80 GMP, 60 PSI and 10 GVF. Similar to horizontal bubbly flows, recognizable air bubbles can be observed in the upstream flow but not in the downstream flow.

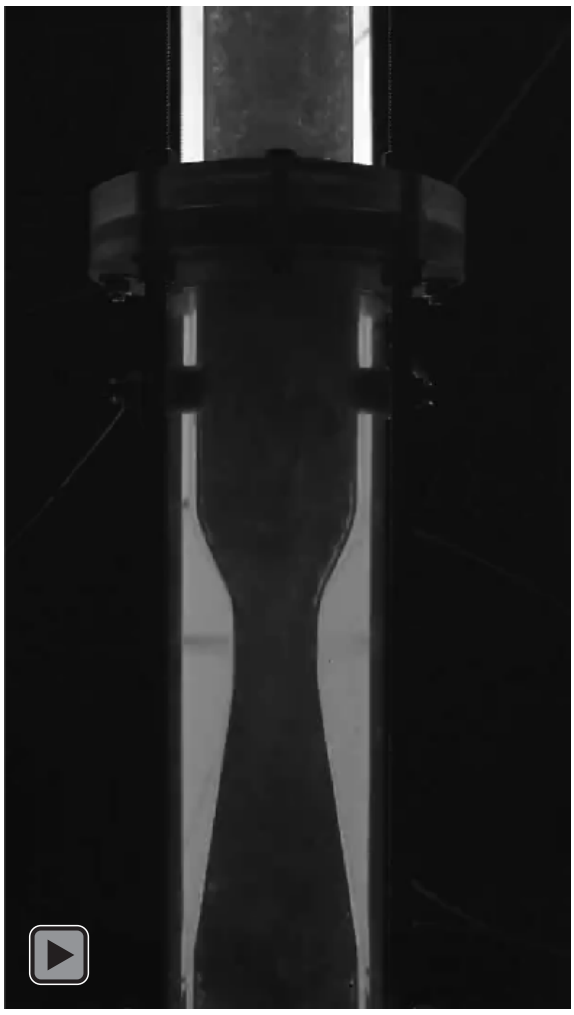

Video 5.5 Vertical bubbly flow at 80 GPM 60 PSI 10 GVF

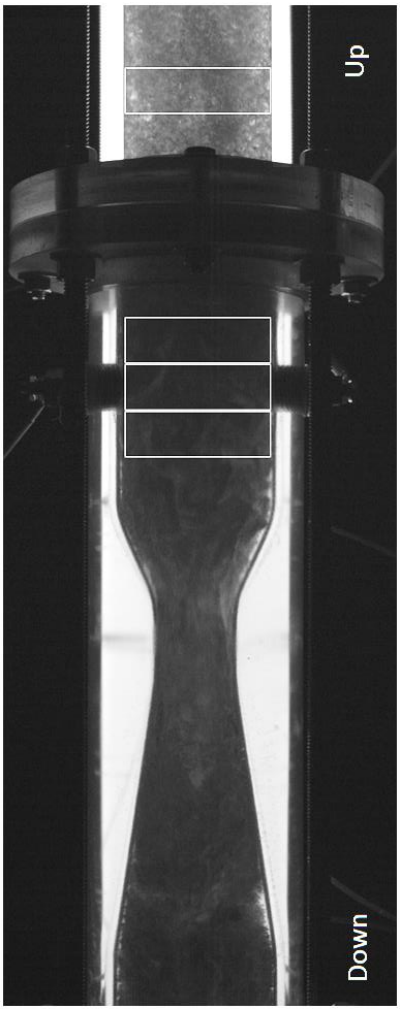


Figure 5.9 Vertical bubbly flow at 80 GPM 60 PSI 10 GVF

As indicated in Figure 5.10, homogenized level and steady level of the flow are dramatically improved with the slotted orifice plate. Peaks of the standard deviation of gray level for upstream flow are mostly conditioned. And flows at 2 inches and 2.5 inches from the plate have similar homogenized level and steadiness. Table 5.23 lists all the actual values of the results.

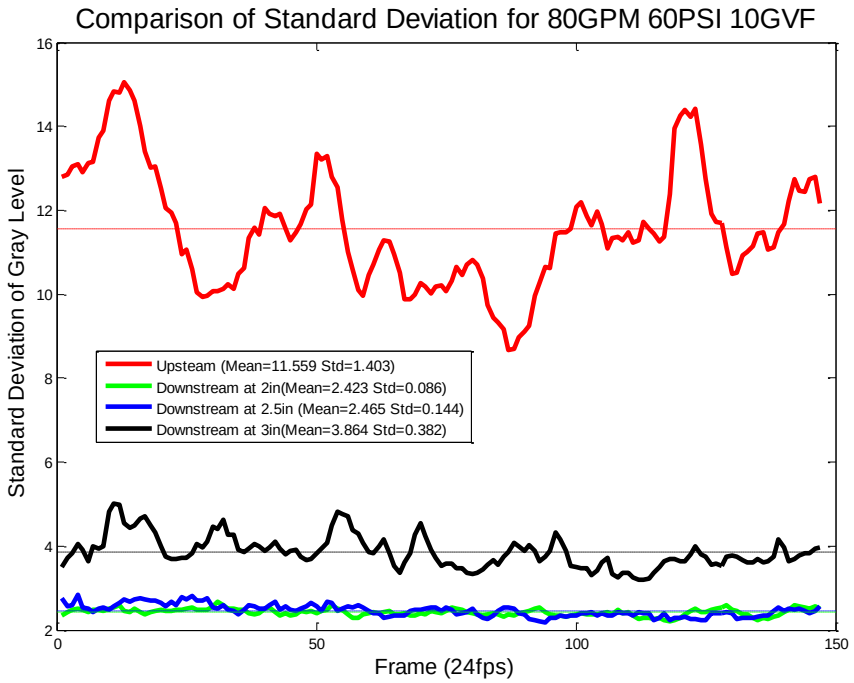


Figure 5.10 Comparison of homogenized level for vertical bubbly flow

Table 5.23 Comparison of homogenized level for vertical bubbly flow

| Zone | Mean | Standard Deviation |
|---|---|---|
| Upstream | 11.559 | 1.403 |
| Downstream 2 in | 2.423 | 0.086 |
| Downstream 2.5 in | 2.465 | 0.144 |
| Downstream 3 in | 3.864 | 0.382 |

### 5.4.2.2 Slug flow

Water slugs and large air bubbles can be seen in the upstream flow when the slug flow shown in Figure 5.11 happens at 50 GPM, 60 PSI and 30 GVF. However, it is still well mixed in the downstream flow by observation.

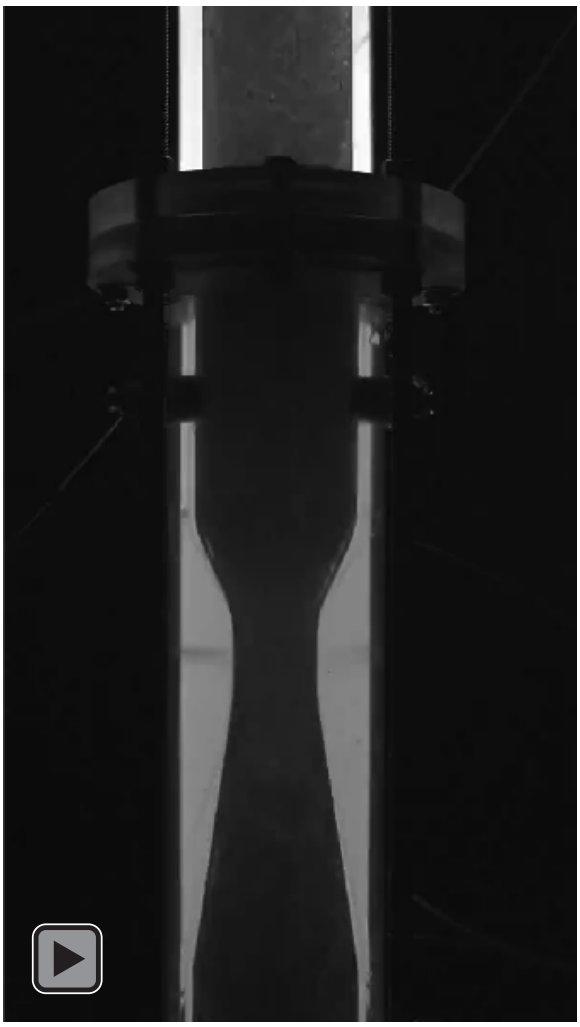

Video 5.6 Vertical slug flow at 50 GPM 60 PSI 30 GVF

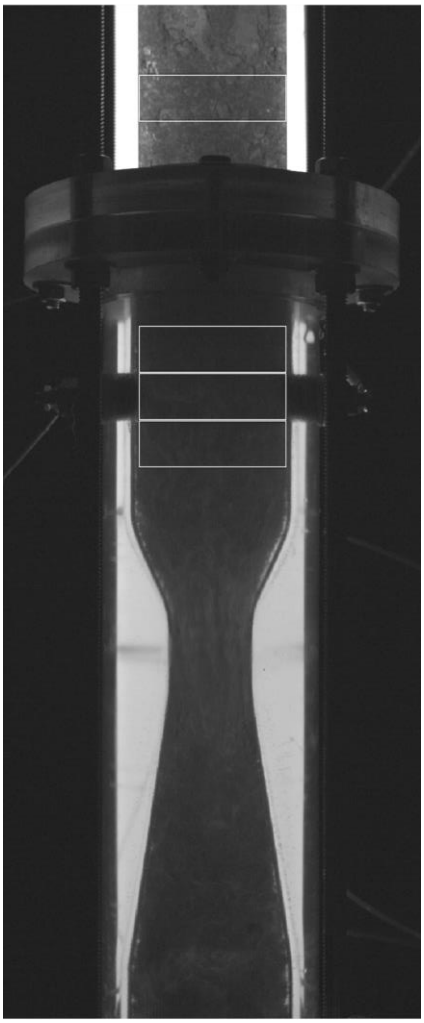

Figure 5.11 Vertical slug flow at 50 GPM 60 PSI 30 GVF

Figure 5.12 shows that the slotted orifice plate has a good homogenize ability for the vertical slug flow. Flows are better mixed and steadier in all three zones than in the upsteam. And flow at 2.5 inches from the plate has higher homogenized level but slightly

lower steadiness than flow at 2 inches from the plate. All the actual values of the results are listed in Table 5.24

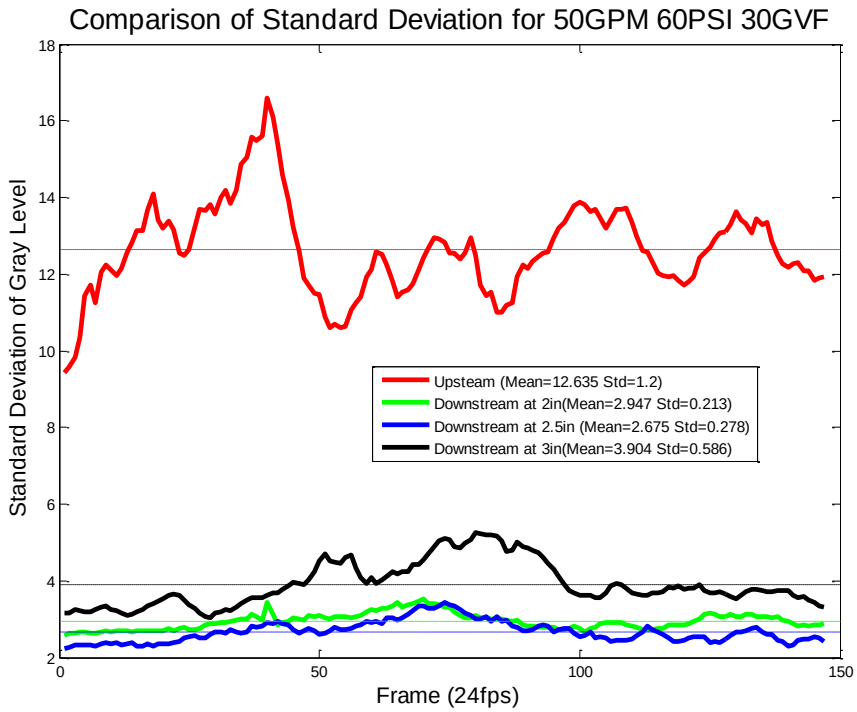


Figure 5.12 Comparison of homogenized level for vertical slug flow

Table 5.24 Comparison of homogenized level for vertical slug flow

| Zone | Mean | Standard Deviation |
|---|---|---|
| Upstream | 12.635 | 1.200 |
| Downstream 2 in | 2.947 | 0.213 |
| Downstream 2.5 in | 2.675 | 0.278 |
| Downstream 3 in | 3.904 | 0.586 |

5.4.2.3 Churn flow

Churn flow shown in Figure 5.13 happens at 30 GPM, 60 PSI and 50 GVF. Churning motions in the upstream as well at in the downstream flow flow can be clearly seen.

Video 5.7 Vertical churn flow at 30 GPM 60 PSI 50 GVF

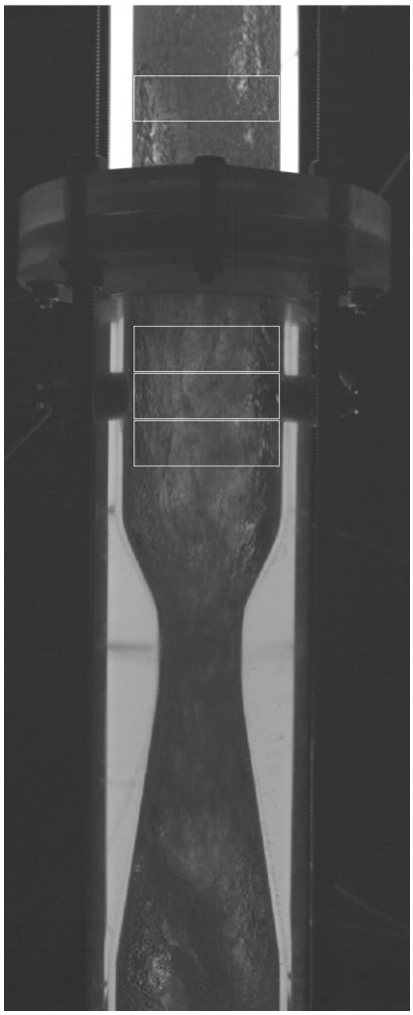

Figure 5.13 Vertical churn flow at 30 GPM 60 PSI 50 GVF

It seems in Figure 5.14 that the slotted orifice cannot compelete get rid of churning motions of the flow, even though there is large improvement in the homogenized level and steadiness of the flow. Among the three zones, flow at 2 inches from the plate are the most homogenized and steady. Table 5.25 lists all the actual values.

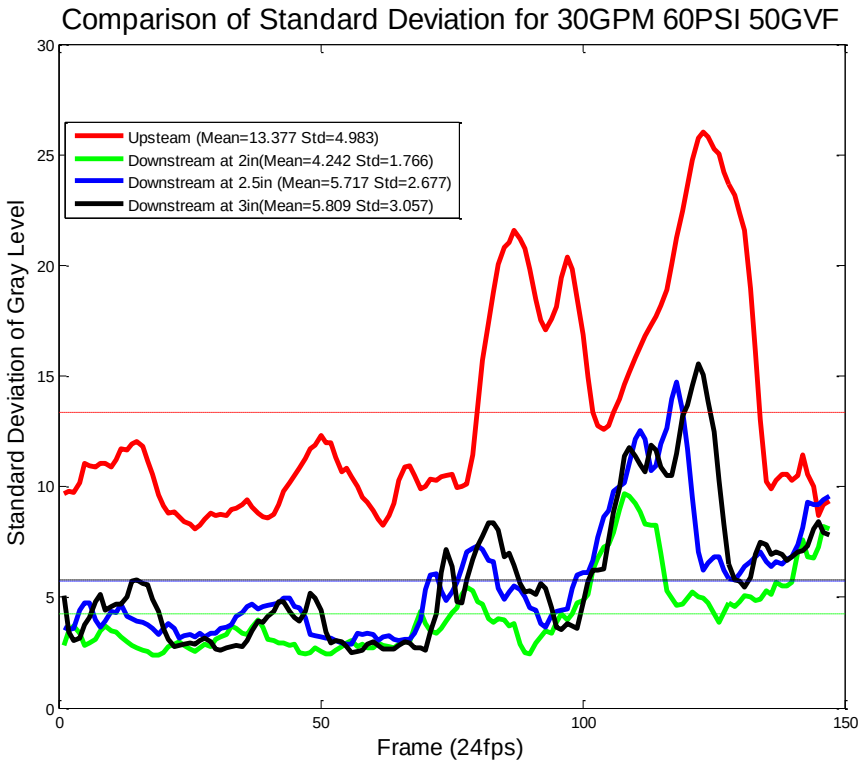


Figure 5.14 Comparison of homogenized level for vertical churn flow

Table 5.25 Comparison of homogenized level for vertical churn flow

| Zone | Mean | Standard Deviation |
|---|---|---|
| Upstream | 13.377 | 4.983 |
| Downstream 2 in | 4.242 | 1.766 |
| Downstream 2.5 in | 5.717 | 2.677 |

Table 5.25 Continued

| | | |
|---|---|---|
| Downstream 3 in | 5.809 | 3.057 |

5.4.2.4 Annular flow

As shown in Figure 5.15, vertical annular flow occurs at 10 GPM, 60 PSI and 97.5 GVF. Water is distrusted evenly along the wall of the pipe and there is an air core at the center part of the pipe carrying only droplets of water.

Video 5.8 Vertical annular flow at 10 GPM 60 PSI 97.5 GVF

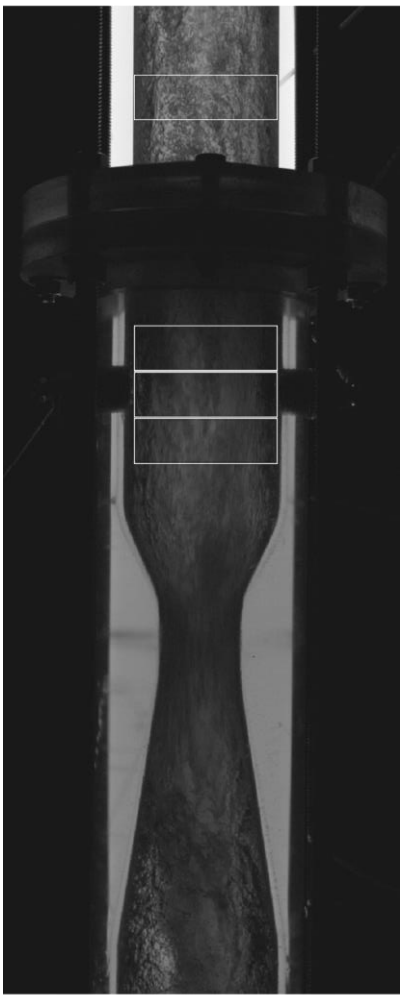

Figure 5.15 Vertical annular flow at 10 GPM 60 PSI 97.5 GVF

Figure 5.16 indicates the ability of the slotted orifice conditioning the mixed flow. The downstream flow is well homogenized and becomes steadier. What is more, since for annular flow, water covers only the outer layer the pipe, flow in the upstream pipe is more chaotic than appeared in the video, which further demonstrates the homogenize ability of the slotted orifice plate. It is also shown that flow at 2 inches from the plate has higher

homogenized level, and flow at 2.5 inches from the plate has higher steadiness. All the actual values of the results are listed in Table 5.26

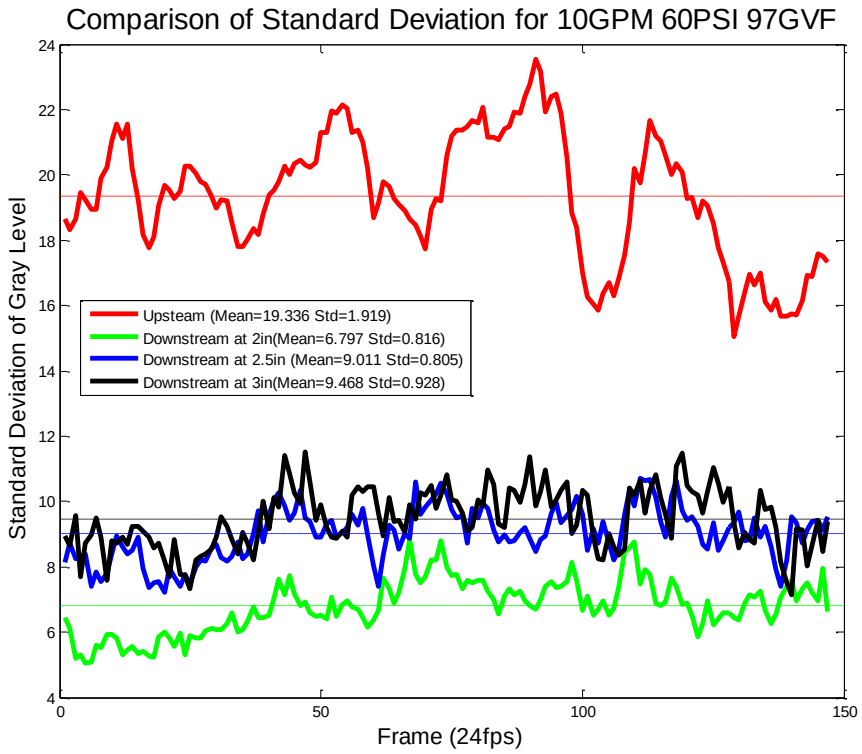


Figure 5.16 Comparison of homogenized level for vertical annular flow

Table 5.26 Comparison of homogenized level for vertical annular flow

| Zone | Mean | Standard Deviation |
|---|---|---|
| Upstream | 19.336 | 1.919 |
| Downstream 2 in | 6.979 | 0.816 |
| Downstream 2.5 in | 9.011 | 0.805 |
| Downstream 3 in | 9.468 | 0.928 |

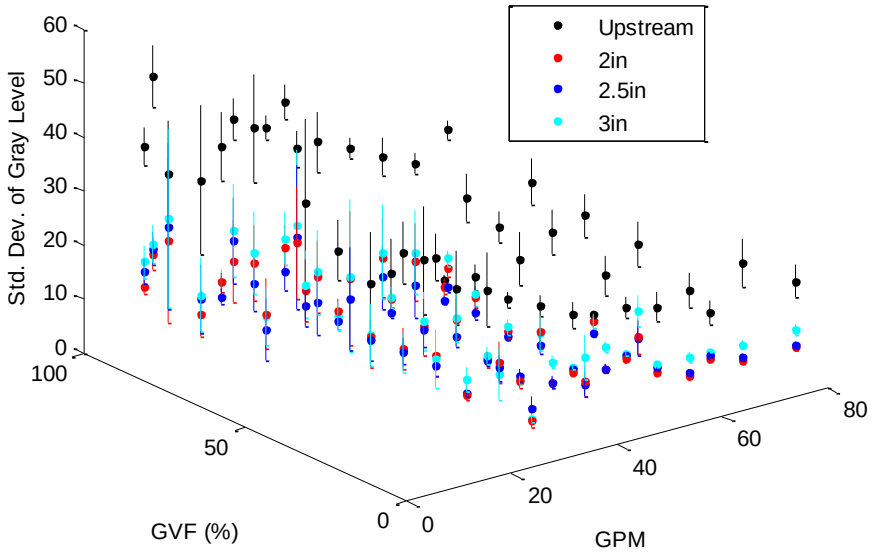


Figure 5.17 Homogenization ability analysis at 60 PSI in horizontal orientation

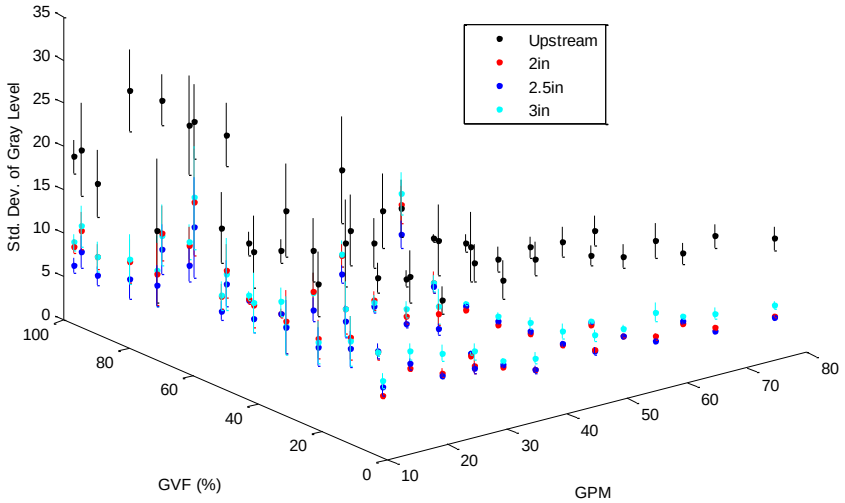


Figure 5.18 Homogenization ability analysis at 60 PSI in vertical orientation

Figure 5.17 and Figure 5.18 Homogenization ability analysis at 60 PSI in vertical orientation are 3D plots of overall homogenization levels at all four sampling spots at various GPM and GVF where the dots indicate the standard deviation of the gray level of a photo (i.e. the homogenization level) and the error bars represent the stability of the homogenization level as time goes. As shown in the figure, the slotted orifice plate has generally very good homogenization ability as a flow conditioner since all red, blue, and cyan dots are below the black dots and the red, blue and cyan error bars are relatively shorter than the black error bars. It also can be found that the error bars are nearly invisible at low GVF while become longer in GVF increases.

A table of all visualization study results is shown in Appendix B.

# 6 CONCLUSION AND RECOMMENDATIONS

## 6.1 Conclusions

The experiment is conducted with the intention of evaluating the effectiveness of the slotted orifice plate multiphase flow meter coupled with Venturi meter, and determine the homogenize ability of the slotted orifice plate with visualization analysis. Water and air mixture is used as the working fluid whose GVF vary from 2.5% to 97.5%.

In this study, the impedance measurement method is proved to be an effective way to measure the GVF of the air-water mixture. The GVF shows a $6^{th}$ order polynomial relationship with the signal gain using 1 MHz signal and a linear relationship with phase angle using 10 MHz signal. In addition, the orientation of the test section is proved no effect on the signal gain measurement, but significantly affects the phase angle measurement.

The study also proves that the bulk flow rate of the mixture can be measured by a simple Venturi pipe. The Discharge Coefficient of the Venturi pipe is 0.97 in horizontal orientation and 0.89 in vertical orientation. The Discharge Coefficient of the Slotted Orifice Plate is not affected by orientation but by GVF, and the lowest Discharge Coefficient occurs at medium GVF.

The visualization study shows that the slotted orifice plate has a good ability to homogenize and stabilize the mixed flow for all flow regimes and for both horizontal and vertical flows. Homogenized level and steadiness of the downstream flow are to a certain extent affected by the flow condition of the upstream flow, and the worst cases are horizontal slug flow and vertical churn flow due to significantly unmixed upstream flows.

## 6.2 Recommendations

In this study, the electrical impedance measurement method has been approved to be effective and accurate in measuring GVF of water-air mixture which is well homogenized by the Slotted Orifice Plate, and the Discharge Coefficients of the Venturi meter in different orientations have been determined. There are still a few recommendations if further studies are going to be conducted in the future.

If water-air mixture is continued to be used as the working fluid, more flow conditions, such as higher flow rates and higher discharge pressures, can be tested in order to widen the known working range of the coupled flow meter.

Different working fluid, such as oil-air mixture and oil-natural gas mixture, can be tested to verify the effectiveness of the flow meter, because for different fluids, the results of electrical impedance measurement and the homogenization ability of the Slotted Orifice Plate may be different.

More data points can be obtained in additional experiments with the purpose of increasing the the accuracy, precision, and repeatability of the results.

Different methods are encouraged to analyze the homogenization ability of the Slotted Orifice Plate, such as using ultrasonic wave and using magnetic field.

# REFERENCES


[1] Thorn, R et al. “Three-Phase Flow Measurement in the Petroleum Industry.” *Measurement Science and Technology*, vol. 24, no. 1, 2012, p. 012003. doi:10.1088/0957-0233/24/1/012003.

[2] "An Introduction to Multiphase Flow Measurement." National Measurement System. Web. 27 April 2016. http://www.tuvnel.com/_x90lbm/An_Introduction_to_Multiphase_Flow_Measurement.pdf

[3] Morrison, Gerald et al. “Evaluation of a Close Coupled Slotted Orifice, Electric Impedance, and Swirl Flow Meters for Multiphase Flow.” *Volume 2, Fora: Cavitation and Multiphase Flow; Fluid Measurements and Instrumentation; Microfluidics; Multiphase Flows: Work in Progress*, July 2013, doi:10.1115/fedsm2013-16112.

[4] Bratland, Ove. *Pipe Flow I Single-phase Flow Assurance*. 2009. Print. ISBN 978-616-335-925-4, www.drbratland.com.

[5] Bratland, Ove. *Pipe flow II Multi-phase Flow Assurance*. 2009. Print. ISBN 978-616-335-926-1, www.drbratland.com.

[6] Da Silva, M. J. (2008). *Impedance sensors for fast multiphase flow measurement and imaging* (Doctoral dissertation). Technische Universtaat Dresden, Dresden, Germany.

[7] "Flow Regimes in Gas-liquid Flows." *Flow Regimes in Gas-liquid Flows*. Web. 20 Apr. 2016. https://www3.nd.edu/~mjm/flow.regimes.html

[8] Cheng, Lixin et al. “Two-Phase Flow Patterns and Flow-Pattern Maps: Fundamentals and Applications.” *Applied Mechanics Reviews*, vol. 61, no. 5, 2008, p. 050802. doi:10.1115/1.2955990.

[9] Mandhane, J.m. et al. “A Flow Pattern Map for Gas—Liquid Flow in Horizontal Pipes.” *International Journal of Multiphase Flow*, vol. 1, no. 4, 1974, pp. 537–553. doi:10.1016/0301-9322(74)90006-8.

[10] Weisman, J., 1983, “Two-Phase Flow Patterns.” Chapter 15 of Handbook of Fluids in Motion, (eds: N.P. Cheremisinoff and R. Gupta), Ann Arbor Science Publ., pp.409~425.

[11] Baker, R. C. *Flow Measurement Handbook: Industrial Designs, Operating Principles, Performance, and Applications*. Cambridge, UK, Cambridge University Press, 2000.

[12] Morrison, G.l. et al. “Comparison of Orifice and Slotted Plate Flowmeters.” *Flow Measurement and Instrumentation*, vol. 5, no. 2, 1994, pp. 71–77. doi:10.1016/0955-5986(94)90039-6.

[13] Ruiz, J. H. (2004). *Low differential pressure and multiphase flow measurements by means of differential pressure devices* (Doctoral dissertation). Texas A&M University, College Station, TX.

[14] Ihfe, L. M. (1994). *Development of the slotted orifice flow conditioner* (Master’s thesis). Texas A&M University, College Station, TX.

[15] Macek, M. L. (1993). *A slotted orifice plate used as a flow measurement device* (Master’s thesis). Texas A&M University, College Station, TX.

[16] Terracina, D. P. (1996). *The experimental and numerical development of the slotted plate, and its design parameter* (Master's thesis). Texas A&M University, College Station, TX.

[17] Brewer, C. V. (1999). *Evaluation of the slotted orifice plate as a two-phase flow meter* (Master's thesis). Texas A&M University, College Station, TX.

[18] Flores, A. E. (2000). *Evaluation of a slotted orifice plate flow meter using horizontal two phase flow* (Master's thesis). Texas A&M University, College Station, TX.

[19] Sparks, S. A. (2004). *Two phase mixing comparison, oil contamination comparison, and manufacturing accuracy effect on calibration of slotted orifice flow meters* (Master's thesis). Texas A&M University, College Station, TX.

[20] Fossa, M. "Design and Performance of a Conductance Probe for Measuring the Liquid Fraction in Two-Phase Gas-Liquid Flows." *Flow Measurement and Instrumentation*, vol. 9, no. 2, 1998, pp. 103–109. doi:10.1016/s0955-5986(98)00011-9.

[21] Andreussi, P., Di Donfransesco, A. D., & Messi, M. (1988). An impedance method for the measurement of liquid hold-up in two-phase flow. *International Journal Multiphase Flow, 14*(6), 777-785.

[22] Andreussi, P. et al. "An Impedance Method for the Measurement of Liquid Hold-up in Two-Phase Flow." *International Journal of Multiphase Flow*, vol. 14, no. 6, 1988, pp. 777–785. doi:10.1016/0301-9322(88)90074-2.

[23] Brook, N. "Flow Measurement of Solid-Liquid Mixtures Using Venturi and Other Meters." *ARCHIVE: Proceedings of the Institution of Mechanical Engineers 1847-*

*1982 (Vols 1-196)*, vol. 176, no. 1962, Jan. 1962, pp. 127–140. doi:10.1243/pime_proc_1962_176_018_02.

[24] Graf, W. H. “A Modified Venturimeter for Measuring Two-Phase Flow or Particle Dynamics and The Venturimeter.” *Journal of Hydraulic Research*, vol. 5, no. 3, 1967, pp. 161–187. doi:10.1080/00221686709500202.

[25] Robinson, M.; Yucel, O.; and Graf, W. H., "Modified venturimeter; a measuring device for solid-liquid mixtures, September 1970" (1970). *Fritz Laboratory Reports.* Paper 1980.
http://preserve.lehigh.edu/engr-civil-environmental-fritz-lab-reports/1980

[26] Shook, C. A., and J. H. Masliyah. “Flow of a Slurry through a Venturi Meter.” *The Canadian Journal of Chemical Engineering*, vol. 52, no. 2, 1974, pp. 228–233. doi:10.1002/cjce.5450520216.

[27] Herringe, R.a. “Slurry Flow Metering by Pressure Differential Devices.” *International Journal of Multiphase Flow*, vol. 3, no. 3, 1977, pp. 285–298. doi:10.1016/0301-9322(77)90008-8.

[28] Hasan, A. Rashid, and Dorab N. Baria. “Pressure Drop and Flow Rate Measurement in Lignite-Water Slurry Flow.” *Energy Sources*, vol. 9, no. 1, 1987, pp. 17–41. doi:10.1080/00908318708908679.

[29] Shook, C. A. “Flow of Stratified Slurries Through Horizontal Venturi Meters.” *The Canadian Journal of Chemical Engineering*, vol. 60, no. 3, 1982, pp. 342–345. doi:10.1002/cjce.5450600303.

[30] Kapoor, B. S. et al. “Discharge Characteristics of Orifice Meters in Sediment-Laden Flows.” *The Canadian Journal of Chemical Engineering*, vol. 64, no. 1, 1986, pp. 36–41. doi:10.1002/cjce.5450640105.

[31] Tiwari, H. L, (1992). *Characteristics of flow through segmental orifice plates for sediment laden water* (Master’s thesis). Maulana Azad National Institute of Technology, Bhopal

[32] Azzopardi, B.j et al. “A Quasi-One-Dimensional Model for Gas/Solids Flow in Venturis.” *Powder Technology*, vol. 102, no. 3, 1999, pp. 281–288. doi:10.1016/s0032-5910(98)00221-6.

[33] Bharani, S et al. “Performance Characteristics of an Eccentric Venturimeter with Elongated Throat for Measurement of Solid-Liquid Flows.” *Indian Journal of Engineering &Amp; Materials Sciences*, vol. 6, June 1999, pp. 119–124.

[34] Miller, Gary. “The Influence of Liquid Viscosity on Multiphase Flow Meters.” 2009, Glasgow, United Kindom, *8th International South East Asia Hydrocarbon Flow Measurement*.

[35] Hollingshead, C.l. et al. “Discharge Coefficient Performance of Venturi, Standard Concentric Orifice Plate, V-Cone and Wedge Flow Meters at Low Reynolds Numbers.” *Journal of Petroleum Science and Engineering*, vol. 78, no. 3-4, 2011, pp. 559–566. doi:10.1016/j.petrol.2011.08.008.

[36] Sihombing, D. J, (2015) *Temperature effect in multiphase flow meter using slotted orifice plate* (Master’s thesis). Texas A&M University, College Station, TX.

[37] *Venturi Meter Calculator*. Digital image. *EFunda*. EFunda, Inc., n.d. Web. 1 Apr. 2016.

# APPENDIX A DRAWINGS OF NON-STANDARD PARTS

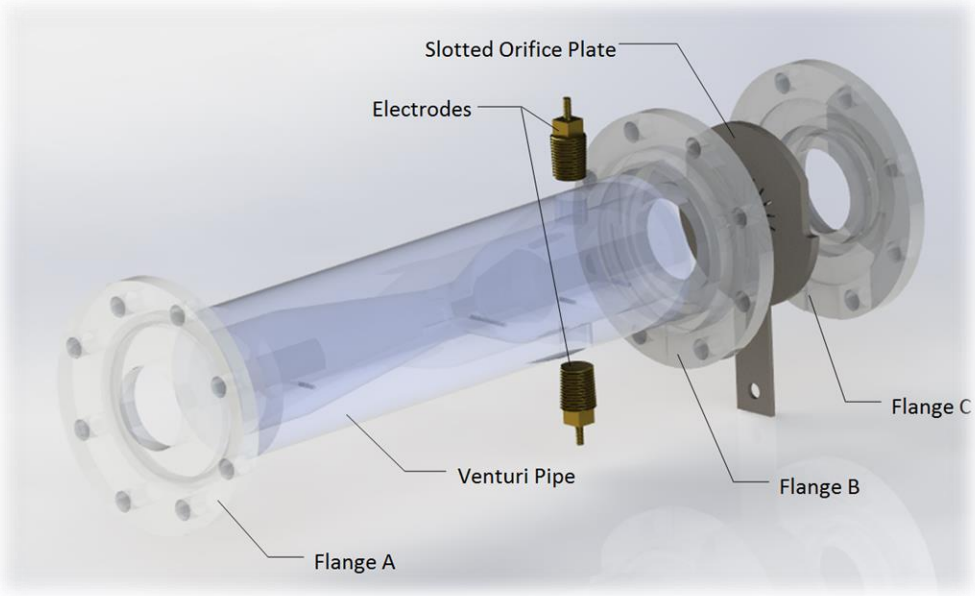


Figure 6.1 Non-standerd parts

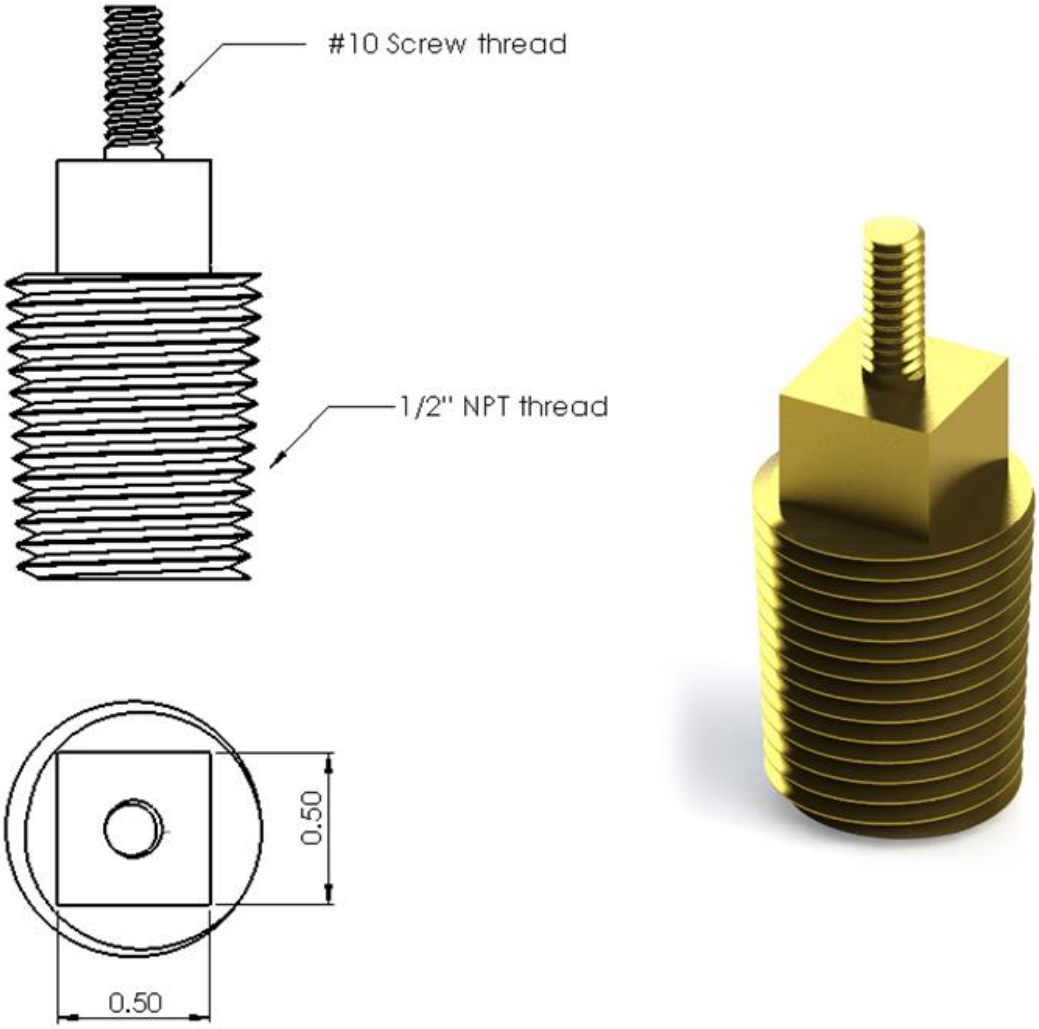


Figure 6.2 Drawing of electrode (ultra-machinable brass)

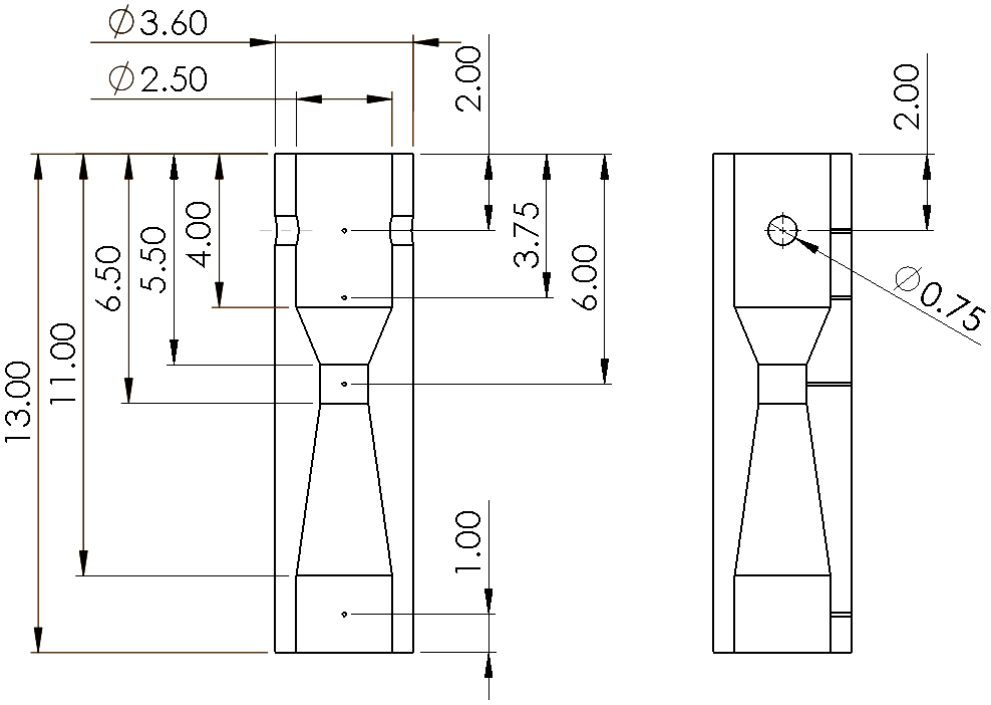


Figure 6.3 Drawing of Venturi pipe (polycarbonate)

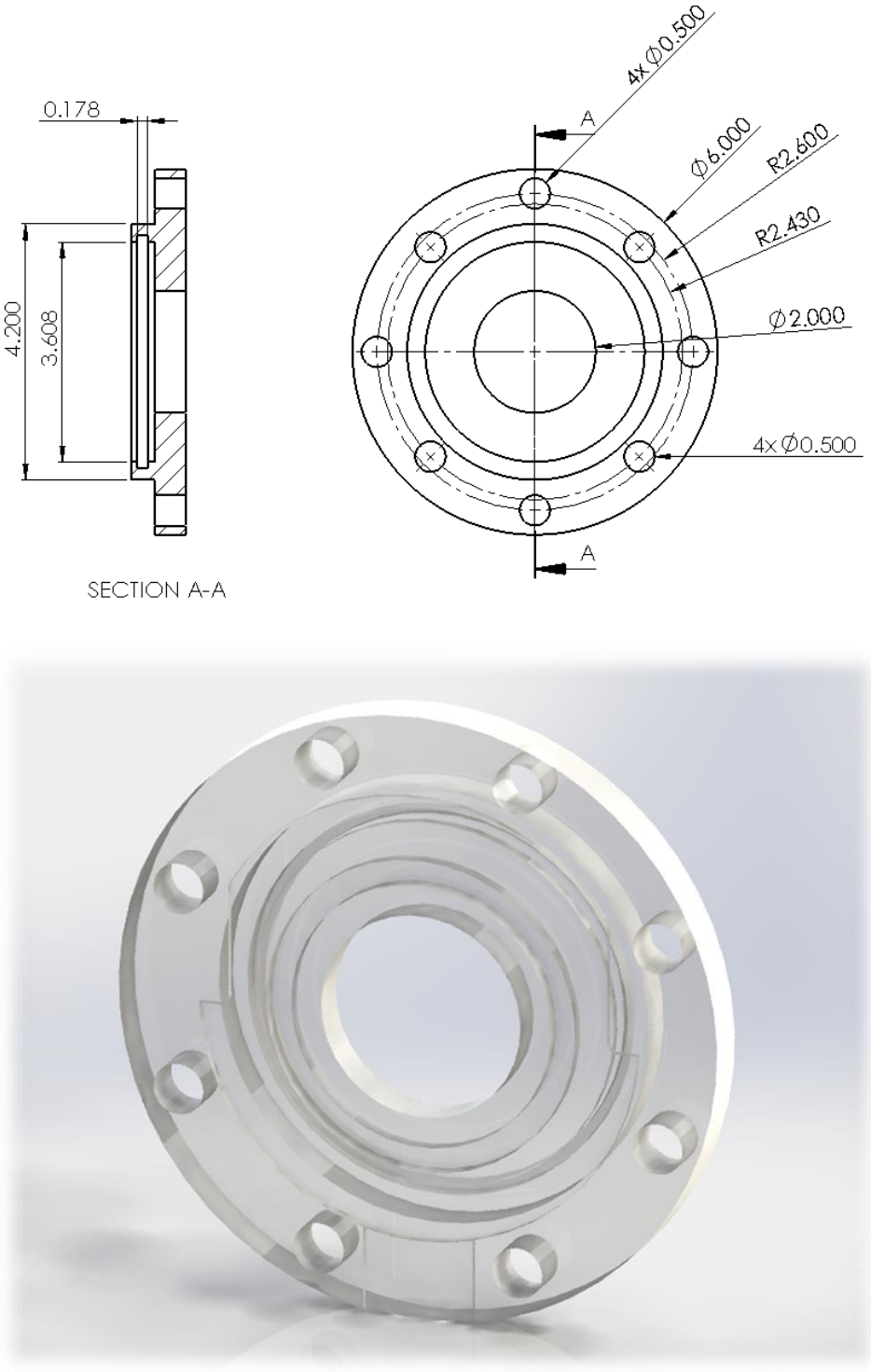


Figure 6.4 Drawing of flange A (polycarbonate)

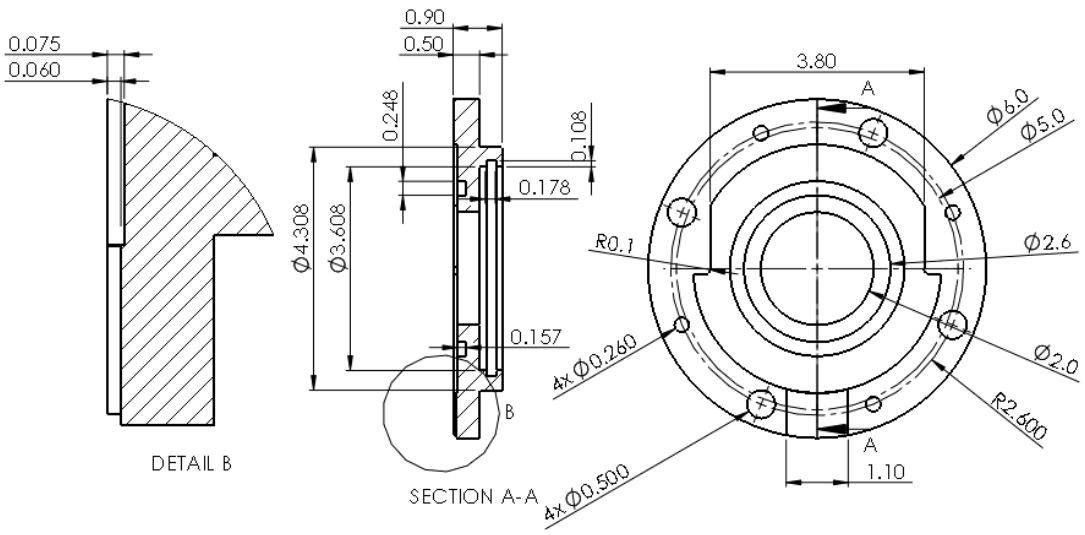


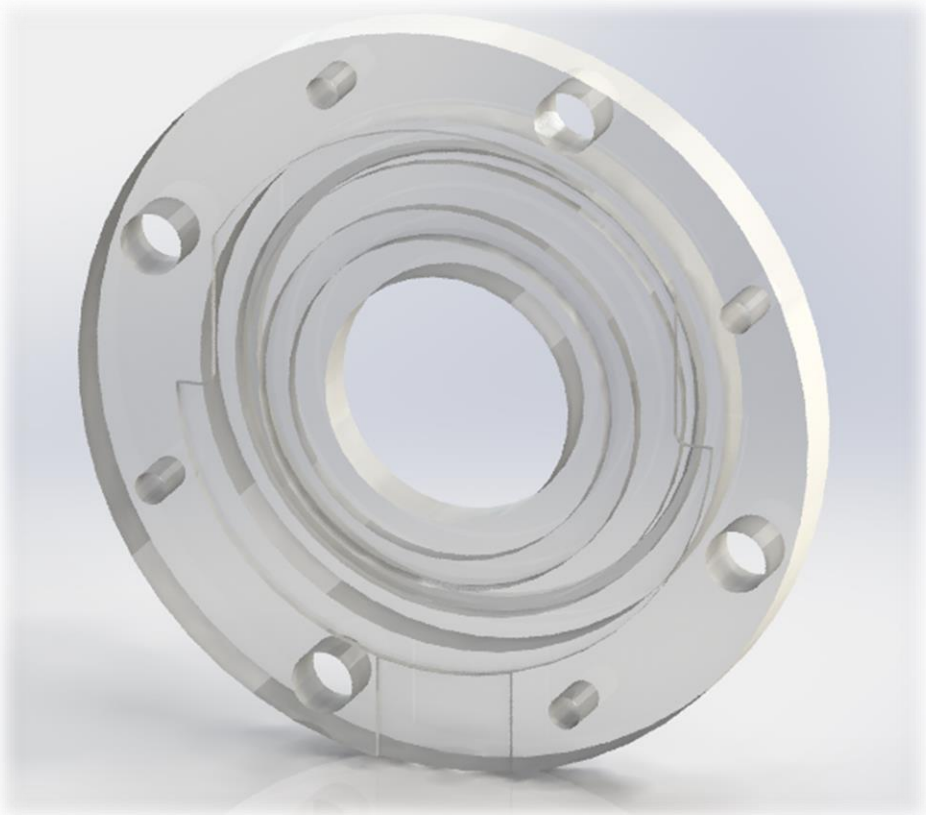

Figure 6.5 Drawing of flange B (polycarbonate)

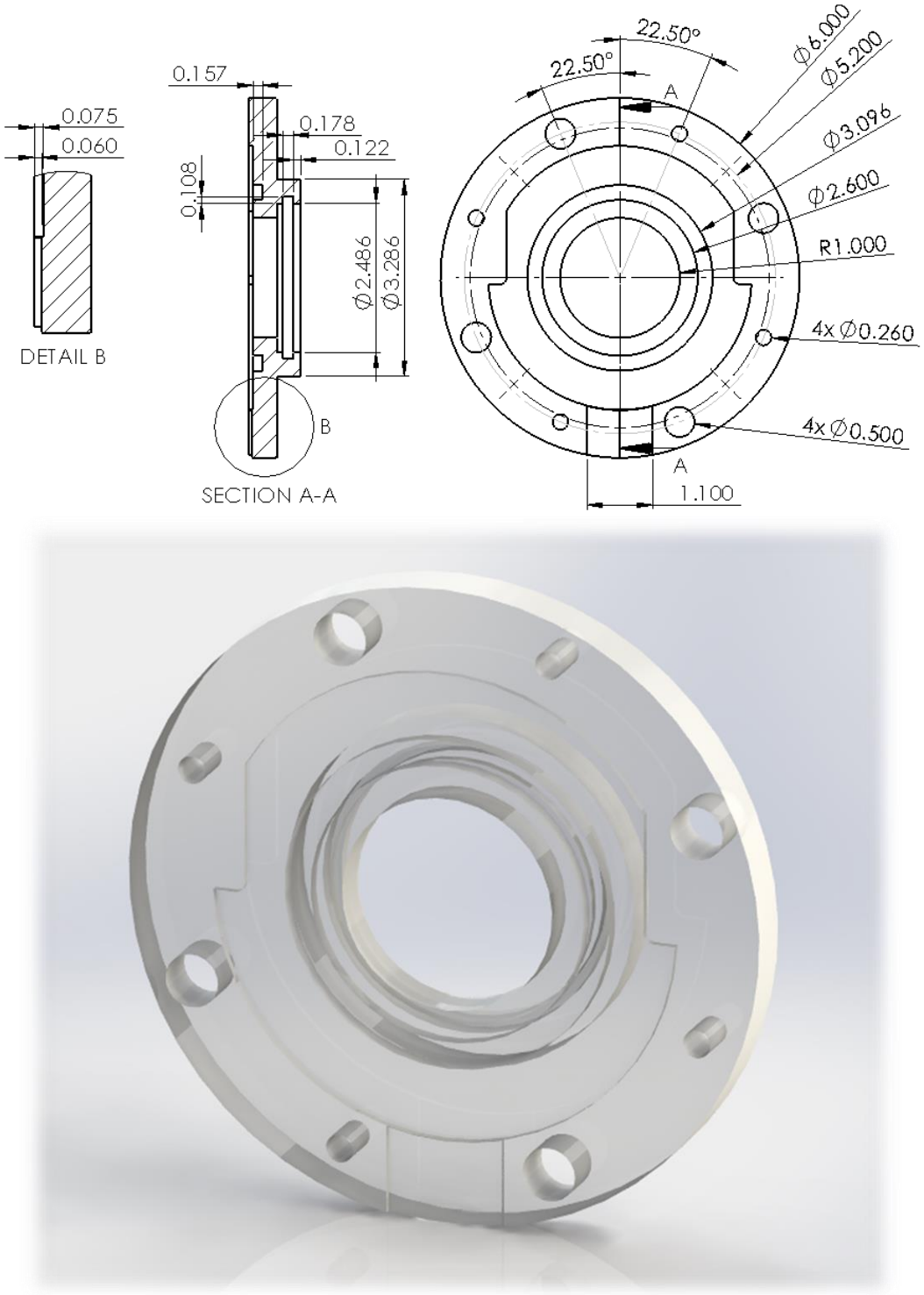


Figure 6.6 Drawing of flange C (polycarbonate)

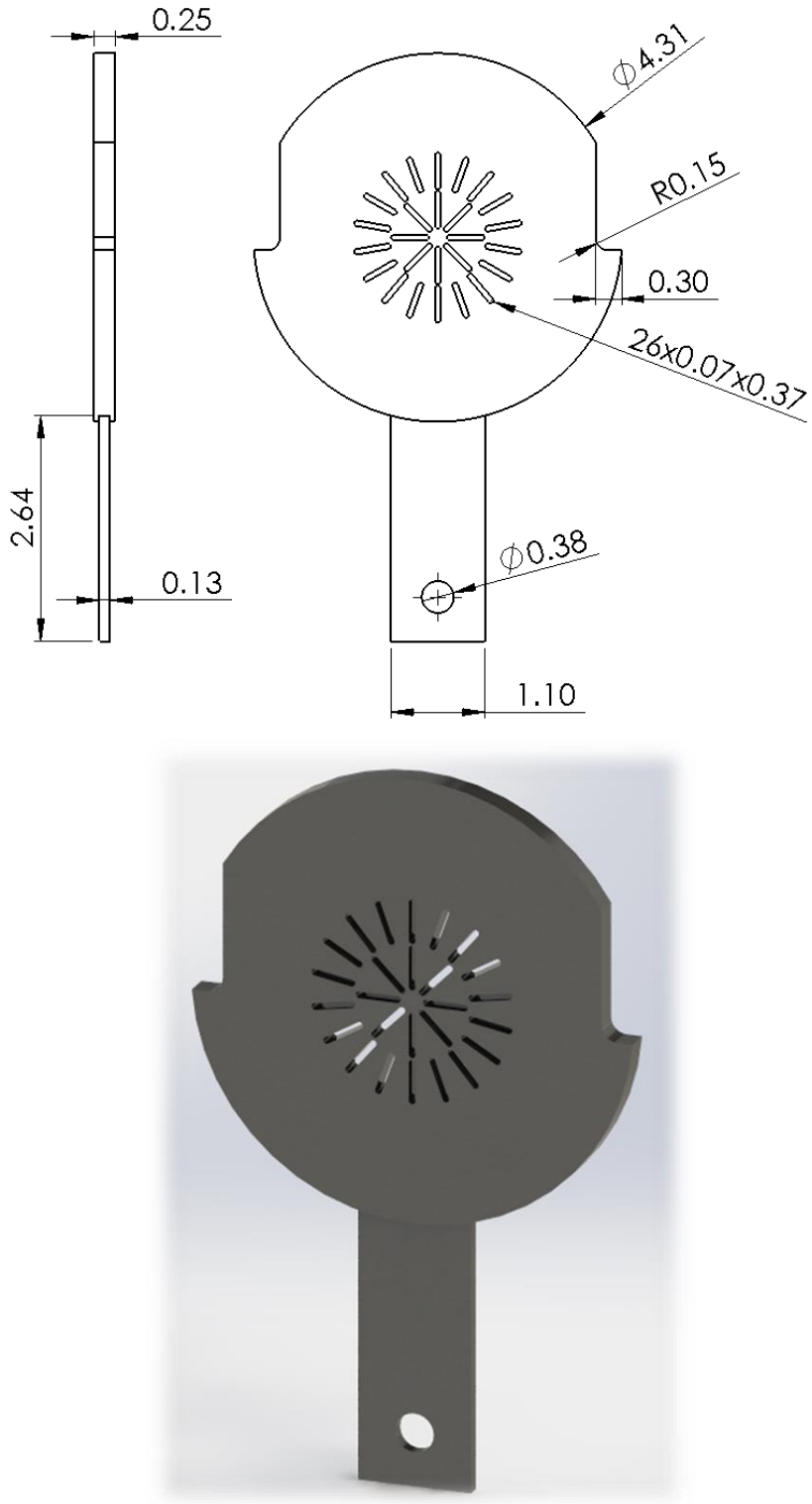


Figure 6.7 Drawing of slotted orifice plate (stainless steel)

# APPENDIX B VISUALIZATION STUDY RESULTS

Table 6.1 Visualization study results
MV=Mean value of standard deviation of gray level
Std=Standard deviation of standard deviation of gray level with respect to time

| Horizontal | | | | | | | | | | |
|---|---|---|---|---|---|---|---|---|---|---|
| GPM | PSI | GVF | Upstream | | 2 in | | 2.5 in | | 3 in | |
| | | | MV | Std | MV | Std | MV | Std | MV | Std |
| 10 | 20 | 50 | 48.65 | 1.37 | 33.80 | 4.87 | 35.03 | 5.19 | 39.07 | 5.46 |
| 10 | 20 | 60 | 48.53 | 2.59 | 17.03 | 5.80 | 20.29 | 7.03 | 22.14 | 7.43 |
| 10 | 20 | 70 | 46.07 | 1.31 | 45.07 | 8.84 | 47.51 | 8.23 | 50.50 | 6.63 |
| 10 | 20 | 80 | 46.32 | 2.32 | 40.91 | 7.76 | 44.88 | 6.86 | 49.85 | 4.80 |
| 10 | 20 | 90 | 41.88 | 10.67 | 13.41 | 3.73 | 16.60 | 3.50 | 18.06 | 3.62 |
| 10 | 20 | 95 | 38.74 | 15.76 | 13.74 | 5.55 | 16.36 | 5.15 | 18.16 | 5.84 |
| 10 | 20 | 96 | 50.47 | 2.54 | 23.01 | 7.04 | 24.75 | 6.43 | 25.87 | 7.12 |
| 10 | 40 | 50 | 43.49 | 11.98 | 30.73 | 8.61 | 35.69 | 9.09 | 39.27 | 10.21 |
| 10 | 40 | 60 | 52.27 | 2.07 | 22.62 | 3.26 | 27.51 | 4.74 | 30.02 | 6.59 |
| 10 | 40 | 70 | 49.13 | 1.89 | 25.64 | 3.91 | 29.27 | 3.59 | 31.93 | 4.13 |
| 10 | 40 | 80 | 49.37 | 1.80 | 33.50 | 9.86 | 28.06 | 9.57 | 42.02 | 8.25 |
| 10 | 40 | 90 | 52.13 | 3.13 | 22.18 | 4.90 | 26.65 | 4.67 | 29.09 | 4.87 |
| 10 | 40 | 95 | 40.77 | 7.86 | 11.10 | 2.89 | 13.96 | 2.81 | 14.71 | 3.04 |
| 10 | 40 | 97.5 | 33.82 | 2.93 | 6.45 | 0.84 | 9.43 | 2.26 | 10.30 | 2.91 |
| 10 | 60 | 50 | 49.03 | 3.28 | 31.80 | 10.55 | 32.68 | 13.39 | 34.99 | 13.87 |
| 10 | 60 | 60 | 50.18 | 2.314 | 15.72 | 6.50 | 12.69 | 5.70 | 15.39 | 5.44 |
| 10 | 60 | 70 | 49.16 | 3.77 | 22.65 | 7.54 | 26.64 | 7.90 | 28.45 | 8.58 |
| 10 | 60 | 80 | 35.01 | 13.87 | 10.16 | 4.27 | 13.09 | 6.37 | 13.7 | 6.89 |
| 10 | 60 | 90 | 33.58 | 9.82 | 21.00 | 15.22 | 23.68 | 15.49 | 25.18 | 16.40 |
| 10 | 60 | 95 | 50.12 | 5.58 | 17.27 | 2.92 | 18.21 | 2.95 | 19.04 | 3.62 |
| 10 | 60 | 97.5 | 36.36 | 3.45 | 10.35 | 1.299 | 13.32 | 2.30 | 15.09 | 2.96 |
| 20 | 20 | 20 | 42.75 | 10.08 | 21.00 | 6.82 | 18.54 | 5.79 | 19.43 | 9.66 |
| 20 | 20 | 30 | 50.01 | 3.36 | 21.84 | 9.84 | 20.46 | 7.08 | 20.68 | 12.55 |
| 20 | 20 | 40 | 50.57 | 2.71 | 30.82 | 6.14 | 27.59 | 6.41 | 33.38 | 6.28 |
| 20 | 20 | 50 | 36.51 | 12.63 | 12.24 | 8.64 | 11.54 | 7.28 | 12.89 | 9.59 |
| 20 | 20 | 60 | 43.73 | 8.59 | 21.56 | 6.95 | 18.76 | 5.75 | 21.97 | 7.88 |
| 20 | 20 | 70 | 26.92 | 16.05 | 10.87 | 5.07 | 9.23 | 4.23 | 11.32 | 5.99 |
| 20 | 20 | 80 | 41.49 | 12.41 | 14.02 | 4.85 | 12.15 | 4.94 | 14.94 | 5.27 |
| 20 | 20 | 90 | 48.59 | 4.22 | 14.90 | 2.37 | 13.06 | 2.10 | 15.60 | 2.55 |
| 20 | 40 | 20 | 47.05 | 4.61 | 16.59 | 6.81 | 15.00 | 6.26 | 16.85 | 6.55 |
| 20 | 40 | 30 | 47.25 | 3.58 | 20.90 | 8.31 | 19.14 | 6.40 | 20.48 | 9.81 |

Table 6.1 Continued Visualization study results

| | | | | | | | | | | |
|---|---|---|---|---|---|---|---|---|---|---|
| 20 | 40 | 40 | 46.57 | 8.32 | 7.48 | 5.49 | 7.39 | 5.31 | 8.24 | 5.01 |
| 20 | 40 | 50 | 48.98 | 3.40 | 30.74 | 8.02 | 27.14 | 8.32 | 34.15 | 9.85 |
| 20 | 40 | 60 | 37.31 | 11.52 | 17.97 | 6.64 | 15.61 | 5.53 | 19.43 | 7.80 |
| 20 | 40 | 70 | 34.84 | 17.25 | 11.28 | 4.29 | 9.38 | 3.74 | 11.87 | 4.83 |
| 20 | 40 | 80 | 50.67 | 5.44 | 20.49 | 5.79 | 16.20 | 4.66 | 22.08 | 6.74 |
| 20 | 40 | 90 | 41.80 | 4.96 | 13.66 | 1.57 | 10.16 | 1.28 | 13.31 | 2.05 |
| 20 | 60 | 20 | 58.24 | 1.76 | 32.47 | 1.64 | 29.04 | 0.82 | 34.37 | 1.41 |
| 20 | 60 | 30 | 49.17 | 1.91 | 30.93 | 7.02 | 26.64 | 5.99 | 32.77 | 7.75 |
| 20 | 60 | 40 | 47.60 | 3.53 | 29.01 | 7.25 | 25.34 | 5.98 | 30.07 | 8.85 |
| 20 | 60 | 50 | 46.64 | 1.88 | 22.43 | 12.42 | 18.51 | 9.50 | 22.75 | 14.14 |
| 20 | 60 | 60 | 44.93 | 5.60 | 19.98 | 6.82 | 15.17 | 5.85 | 20.82 | 7.72 |
| 20 | 60 | 70 | 49.62 | 3.09 | 22.53 | 4.28 | 18.25 | 3.62 | 24.34 | 4.81 |
| 20 | 60 | 80 | 42.00 | 9.99 | 17.09 | 7.07 | 13.35 | 5.28 | 18.84 | 7.58 |
| 20 | 60 | 90 | 35.79 | 6.36 | 10.71 | 1.82 | 7.99 | 1.45 | 10.92 | 2.16 |
| 30 | 20 | 20 | 45.28 | 5.40 | 26.48 | 5.99 | 20.46 | 4.23 | 28.24 | 7.36 |
| 30 | 20 | 30 | 44.36 | 6.24 | 15.22 | 9.15 | 12.84 | 5.40 | 14.21 | 11.12 |
| 30 | 20 | 50 | 28.47 | 12.85 | 10.03 | 2.02 | 7.55 | 1.46 | 8.93 | 2.18 |
| 30 | 20 | 60 | 25.87 | 13.51 | 9.15 | 4.63 | 6.95 | 3.19 | 9.10 | 5.00 |
| 30 | 40 | 20 | 43.99 | 3.32 | 7.34 | 4.45 | 7.81 | 3.81 | 7.45 | 2.22 |
| 30 | 40 | 30 | 43.27 | 4.03 | 7.01 | 2.02 | 6.73 | 1.27 | 5.74 | 1.94 |
| 30 | 40 | 40 | 39.07 | 8.31 | 14.01 | 5.27 | 10.59 | 3.84 | 13.43 | 6.77 |
| 30 | 40 | 50 | 29.77 | 12.17 | 13.37 | 5.58 | 9.76 | 3.51 | 13.70 | 6.29 |
| 30 | 40 | 60 | 42.78 | 15.04 | 12.83 | 7.49 | 10.22 | 5.39 | 13.16 | 8.85 |
| 30 | 40 | 70 | 27.37 | 9.55 | 10.76 | 3.20 | 7.36 | 2.03 | 11.48 | 3.89 |
| 30 | 40 | 80 | 24.76 | 15.55 | 9.33 | 5.57 | 7.04 | 4.12 | 9.47 | 5.75 |
| 30 | 60 | 10 | 48.62 | 4.30 | 4.31 | 1.31 | 6.49 | 2.38 | 4.82 | 0.79 |
| 30 | 60 | 20 | 37.58 | 2.93 | 12.58 | 3.85 | 11.38 | 2.42 | 10.28 | 4.84 |
| 30 | 60 | 30 | 40.33 | 4.46 | 3.63 | 0.94 | 4.11 | 0.80 | 6.55 | 2.22 |
| 30 | 60 | 40 | 26.49 | 4.26 | 8.37 | 4.00 | 6.46 | 1.89 | 7.67 | 5.36 |
| 30 | 60 | 50 | 24.63 | 5.71 | 6.79 | 3.84 | 6.28 | 2.51 | 6.03 | 3.70 |
| 30 | 60 | 60 | 16.19 | 9.51 | 6.31 | 5.93 | 5.50 | 3.56 | 6.56 | 5.85 |
| 30 | 60 | 70 | 19.51 | 5.41 | 8.34 | 2.28 | 6.38 | 1.65 | 7.30 | 2.47 |
| 30 | 60 | 80 | 25.44 | 15.72 | 9.32 | 5.80 | 6.38 | 3.60 | 10.32 | 6.23 |
| 40 | 20 | 10 | 27.13 | 5.25 | 2.94 | 0.24 | 3.41 | 0.25 | 4.48 | 0.60 |
| 40 | 20 | 20 | 25.60 | 2.96 | 7.94 | 1.32 | 5.99 | 0.88 | 7.64 | 1.65 |
| 40 | 20 | 30 | 21.40 | 4.99 | 7.23 | 3.04 | 5.67 | 2.06 | 7.28 | 3.00 |
| 40 | 40 | 10 | 28.30 | 4.51 | 4.68 | 0.45 | 4.79 | 0.36 | 8.04 | 0.90 |
| 40 | 40 | 20 | 26.45 | 4.22 | 3.43 | 0.41 | 4.04 | 0.87 | 5.87 | 1.11 |
| 40 | 40 | 30 | 18.48 | 2.59 | 3.60 | 0.59 | 3.94 | 0.38 | 3.82 | 0.59 |
| 40 | 40 | 40 | 20.33 | 3.12 | 4.31 | 0.75 | 4.04 | 0.66 | 4.41 | 0.68 |

Table 6.1 Continued Visualization study results

| | | | | | | | | | | |
|---|---|---|---|---|---|---|---|---|---|---|
| 40 | 40 | 50 | 17.17 | 5.68 | 7.08 | 3.79 | 5.24 | 2.34 | 8.32 | 3.86 |
| 40 | 40 | 60 | 15.69 | 3.68 | 3.26 | 0.56 | 4.26 | 0.56 | 4.49 | 1.28 |
| 40 | 40 | 70 | 18.17 | 5.66 | 7.09 | 1.46 | 4.71 | 0.63 | 8.60 | 1.93 |
| 40 | 60 | 10 | 39.77 | 3.91 | 8.98 | 2.83 | 8.49 | 2.18 | 13.67 | 4.13 |
| 40 | 60 | 20 | 33.91 | 4.08 | 6.00 | 0.93 | 6.14 | 1.13 | 9.90 | 1.16 |
| 40 | 60 | 30 | 26.17 | 4.92 | 3.66 | 1.31 | 4.62 | 1.12 | 3.78 | 0.70 |
| 40 | 60 | 40 | 17.82 | 6.83 | 4.86 | 1.37 | 4.51 | 0.75 | 5.63 | 1.50 |
| 40 | 60 | 50 | 15.34 | 6.86 | 9.68 | 3.52 | 6.43 | 1.92 | 9.89 | 4.42 |
| 40 | 60 | 60 | 17.75 | 9.99 | 5.40 | 5.24 | 4.89 | 3.27 | 6.48 | 5.51 |
| 40 | 60 | 70 | 12.58 | 6.37 | 7.81 | 1.55 | 5.20 | 1.00 | 8.14 | 1.87 |
| 50 | 40 | 10 | 25.94 | 3.78 | 7.51 | 0.84 | 6.69 | 0.84 | 11.97 | 1.28 |
| 50 | 40 | 20 | 19.15 | 3.59 | 2.84 | 0.21 | 3.44 | 0.14 | 4.45 | 0.38 |
| 50 | 40 | 30 | 18.62 | 7.03 | 4.97 | 2.29 | 4.34 | 1.56 | 4.59 | 2.22 |
| 50 | 40 | 40 | 10.18 | 1.46 | 3.90 | 0.74 | 3.53 | 0.37 | 4.99 | 1.36 |
| 50 | 60 | 10 | 31.95 | 4.07 | 14.66 | 3.16 | 14.42 | 3.08 | 19.51 | 2.90 |
| 50 | 60 | 20 | 23.29 | 3.74 | 6.02 | 0.82 | 6.08 | 0.73 | 10.01 | 1.04 |
| 50 | 60 | 30 | 13.23 | 2.28 | 2.46 | 0.09 | 3.24 | 0.08 | 3.55 | 0.23 |
| 50 | 60 | 40 | 12.16 | 1.79 | 7.30 | 3.08 | 4.98 | 1.71 | 7.15 | 3.26 |
| 50 | 60 | 50 | 10.59 | 1.43 | 4.63 | 1.20 | 3.65 | 0.44 | 5.54 | 1.42 |
| 50 | 60 | 60 | 12.00 | 2.35 | 8.28 | 1.87 | 5.38 | 1.13 | 9.05 | 2.31 |
| 50 | 60 | 70 | 8.69 | 0.90 | 7.56 | 1.52 | 5.04 | 0.73 | 7.58 | 1.96 |
| 60 | 40 | 10 | 22.99 | 3.90 | 6.96 | 0.83 | 6.45 | 0.89 | 11.39 | 1.10 |
| 60 | 40 | 20 | 13.83 | 2.44 | 2.79 | 0.28 | 3.29 | 0.16 | 4.24 | 0.50 |
| 60 | 60 | 10 | 20.63 | 3.12 | 4.90 | 0.46 | 5.54 | 0.56 | 8.22 | 0.92 |
| 60 | 60 | 20 | 14.81 | 2.73 | 2.76 | 0.14 | 3.55 | 0.11 | 4.36 | 0.25 |
| 60 | 60 | 30 | 12.09 | 1.92 | 2.30 | 0.10 | 3.05 | 0.08 | 3.36 | 0.21 |
| 60 | 60 | 40 | 8.03 | 0.65 | 6.70 | 1.16 | 4.47 | 0.67 | 6.65 | 1.30 |
| 70 | 60 | 10 | 23.09 | 4.35 | 4.91 | 0.50 | 5.57 | 0.62 | 7.95 | 0.74 |
| 70 | 60 | 20 | 11.20 | 2.27 | 2.68 | 0.14 | 3.30 | 0.14 | 3.96 | 0.24 |
| 80 | 60 | 10 | 16.99 | 3.02 | 4.78 | 0.55 | 5.25 | 0.67 | 8.02 | 0.98 |

Vertical

| GPM | PSI | GVF | Upstream | | 2 in | | 2.5 in | | 3 in | |
|---|---|---|---|---|---|---|---|---|---|---|
| | | | MV | Std | MV | Std | MV | Std | MV | Std |
| 10 | 20 | 50 | 26.09 | 7.07 | 13.65 | 4.61 | 11.49 | 4.27 | 13.46 | 4.80 |
| 10 | 20 | 60 | 23.47 | 6.61 | 15.60 | 2.15 | 13.39 | 1.66 | 14.81 | 2.63 |
| 10 | 20 | 70 | 21.75 | 7.06 | 16.73 | 3.84 | 14.42 | 2.48 | 16.92 | 5.37 |
| 10 | 20 | 80 | 19.82 | 4.13 | 13.28 | 2.70 | 11.12 | 2.11 | 13.37 | 3.17 |
| 10 | 20 | 90 | 27.62 | 5.53 | 15.38 | 3.36 | 13.44 | 3.50 | 15.94 | 3.20 |

Table 6.1 Continued Visualization study results

| | | | | | | | | | | |
|---|---|---|---|---|---|---|---|---|---|---|
| 10 | 20 | 95 | 20.85 | 8.65 | 15.90 | 8.43 | 13.95 | 8.13 | 16.94 | 9.54 |
| 10 | 40 | 50 | 35.77 | 2.34 | 28.43 | 3.39 | 27.00 | 3.56 | 28.77 | 3.33 |
| 10 | 40 | 60 | 31.98 | 5.74 | 15.44 | 4.22 | 13.47 | 3.71 | 15.25 | 4.61 |
| 10 | 40 | 70 | 20.26 | 5.89 | 9.93 | 2.86 | 8.33 | 2.55 | 9.51 | 2.93 |
| 10 | 40 | 80 | 33.35 | 3.28 | 16.12 | 4.25 | 14.56 | 4.43 | 16.01 | 4.41 |
| 10 | 40 | 90 | 31.87 | 4.16 | 17.58 | 3.35 | 15.75 | 3.52 | 17.73 | 3.59 |
| 10 | 40 | 95 | 32.34 | 1.70 | 18.36 | 2.60 | 15.93 | 2.75 | 19.35 | 2.38 |
| 10 | 40 | 97 | 19.22 | 3.74 | 8.43 | 1.13 | 6.46 | 0.95 | 8.62 | 1.13 |
| 10 | 60 | 50 | 29.44 | 3.65 | 13.72 | 3.10 | 12.27 | 2.65 | 13.37 | 4.16 |
| 10 | 60 | 60 | 29.31 | 4.26 | 20.03 | 6.14 | 17.15 | 5.79 | 20.59 | 5.95 |
| 10 | 60 | 70 | 30.23 | 2.89 | 14.87 | 3.20 | 13.02 | 2.85 | 14.62 | 3.51 |
| 10 | 60 | 80 | 29.71 | 4.78 | 10.04 | 2.46 | 7.92 | 2.17 | 10.30 | 2.85 |
| 10 | 60 | 90 | 17.35 | 3.90 | 8.96 | 1.47 | 6.78 | 1.09 | 8.98 | 1.69 |
| 10 | 60 | 95 | 20.50 | 5.36 | 11.16 | 2.12 | 8.66 | 1.85 | 11.70 | 2.35 |
| 10 | 60 | 97 | 19.34 | 1.92 | 9.01 | 0.80 | 6.80 | 0.82 | 9.47 | 0.93 |
| 20 | 20 | 20 | 25.32 | 4.74 | 14.43 | 3.81 | 11.68 | 3.22 | 14.37 | 4.30 |
| 20 | 20 | 30 | 27.10 | 3.75 | 15.31 | 3.87 | 12.83 | 3.27 | 15.32 | 4.34 |
| 20 | 20 | 40 | 24.91 | 4.46 | 13.26 | 3.05 | 11.19 | 2.36 | 12.90 | 3.30 |
| 20 | 20 | 50 | 29.09 | 6.93 | 15.11 | 4.80 | 12.51 | 4.68 | 15.22 | 5.20 |
| 20 | 20 | 60 | 13.95 | 1.93 | 6.39 | 0.89 | 5.97 | 0.71 | 5.39 | 0.72 |
| 20 | 20 | 70 | 27.39 | 6.82 | 17.39 | 6.88 | 14.61 | 6.55 | 18.62 | 7.46 |
| 20 | 20 | 80 | 12.51 | 5.48 | 6.46 | 2.11 | 4.92 | 1.44 | 6.65 | 2.46 |
| 20 | 20 | 90 | 21.28 | 5.51 | 8.97 | 2.04 | 6.75 | 1.73 | 9.42 | 2.33 |
| 20 | 40 | 20 | 13.30 | 3.97 | 8.06 | 2.35 | 7.07 | 1.67 | 7.37 | 2.82 |
| 20 | 40 | 30 | 15.21 | 3.78 | 7.64 | 2.23 | 6.41 | 1.68 | 7.04 | 2.72 |
| 20 | 40 | 40 | 12.77 | 5.53 | 7.13 | 1.72 | 6.38 | 1.38 | 5.84 | 1.84 |
| 20 | 40 | 50 | 16.13 | 5.22 | 3.41 | 2.42 | 3.90 | 1.90 | 3.11 | 1.72 |
| 20 | 40 | 60 | 17.16 | 7.63 | 12.61 | 7.10 | 10.92 | 6.09 | 13.44 | 8.31 |
| 20 | 40 | 70 | 14.78 | 6.33 | 5.64 | 1.83 | 4.28 | 1.29 | 6.01 | 2.08 |
| 20 | 40 | 80 | 18.76 | 7.11 | 9.63 | 2.59 | 7.55 | 2.35 | 10.05 | 2.85 |
| 20 | 40 | 90 | 16.21 | 3.34 | 5.54 | 0.88 | 3.80 | 0.53 | 5.68 | 1.09 |
| 20 | 60 | 20 | 23.71 | 4.32 | 2.44 | 0.28 | 3.47 | 1.05 | 4.08 | 0.88 |
| 20 | 60 | 30 | 19.88 | 4.01 | 7.46 | 2.45 | 6.17 | 2.06 | 7.11 | 2.87 |
| 20 | 60 | 40 | 12.10 | 3.73 | 5.70 | 2.28 | 4.83 | 2.16 | 5.37 | 2.40 |
| 20 | 60 | 50 | 18.94 | 5.32 | 6.13 | 3.62 | 5.47 | 3.07 | 5.65 | 3.38 |
| 20 | 60 | 60 | 12.53 | 4.14 | 6.44 | 2.64 | 4.79 | 1.51 | 6.69 | 3.43 |
| 20 | 60 | 70 | 13.75 | 4.12 | 5.78 | 1.40 | 4.17 | 1.06 | 5.91 | 1.69 |
| 20 | 60 | 80 | 23.94 | 5.72 | 10.15 | 2.12 | 7.83 | 1.94 | 10.53 | 2.00 |
| 20 | 60 | 90 | 10.17 | 8.26 | 5.18 | 3.53 | 3.85 | 2.40 | 5.55 | 4.03 |
| 30 | 20 | 20 | 17.23 | 4.66 | 6.56 | 2.49 | 4.97 | 1.72 | 6.69 | 2.64 |

Table 6.1 Continued Visualization study results

| | | | | | | | | | | |
|---|---|---|---|---|---|---|---|---|---|---|
| 30 | 20 | 30 | 17.22 | 6.20 | 6.72 | 2.18 | 5.58 | 1.65 | 6.62 | 2.81 |
| 30 | 20 | 40 | 13.74 | 5.13 | 5.68 | 2.37 | 4.48 | 1.51 | 5.31 | 2.82 |
| 30 | 20 | 50 | 15.35 | 4.94 | 5.02 | 1.47 | 4.22 | 1.00 | 4.35 | 1.57 |
| 30 | 20 | 60 | 28.38 | 4.47 | 16.21 | 3.59 | 13.87 | 3.49 | 17.00 | 3.57 |
| 30 | 40 | 20 | 9.54 | 1.43 | 2.15 | 0.50 | 2.48 | 0.88 | 3.09 | 0.63 |
| 30 | 40 | 30 | 19.16 | 4.71 | 5.21 | 2.05 | 4.56 | 1.38 | 4.48 | 2.28 |
| 30 | 40 | 40 | 12.02 | 3.84 | 5.35 | 1.10 | 4.41 | 0.79 | 5.08 | 1.42 |
| 30 | 40 | 50 | 9.17 | 1.69 | 3.10 | 1.11 | 2.59 | 0.71 | 3.13 | 1.24 |
| 30 | 40 | 60 | 23.90 | 3.93 | 10.05 | 2.55 | 7.90 | 2.36 | 10.51 | 2.69 |
| 30 | 40 | 70 | 7.25 | 2.18 | 2.80 | 0.55 | 2.14 | 0.34 | 3.13 | 0.71 |
| 30 | 40 | 80 | 7.17 | 1.80 | 3.94 | 1.21 | 2.74 | 0.62 | 4.53 | 1.71 |
| 30 | 60 | 10 | 17.56 | 2.13 | 5.65 | 0.80 | 5.36 | 0.61 | 7.34 | 0.93 |
| 30 | 60 | 20 | 11.65 | 1.53 | 3.26 | 0.48 | 2.99 | 0.39 | 5.57 | 0.87 |
| 30 | 60 | 30 | 12.70 | 3.00 | 2.22 | 0.31 | 2.69 | 0.60 | 4.13 | 0.95 |
| 30 | 60 | 40 | 11.03 | 1.72 | 2.37 | 0.73 | 2.60 | 0.90 | 2.38 | 0.44 |
| 30 | 60 | 50 | 13.38 | 4.98 | 5.79 | 2.74 | 4.38 | 1.85 | 5.85 | 3.11 |
| 30 | 60 | 60 | 11.01 | 3.63 | 6.20 | 2.12 | 4.16 | 1.33 | 6.12 | 2.20 |
| 30 | 60 | 70 | 9.29 | 1.32 | 2.11 | 0.51 | 2.00 | 0.14 | 3.44 | 1.60 |
| 30 | 60 | 80 | 8.56 | 1.32 | 2.15 | 0.60 | 2.08 | 0.25 | 2.56 | 0.51 |
| 40 | 20 | 10 | 17.56 | 1.53 | 4.63 | 0.48 | 4.84 | 0.77 | 6.85 | 0.73 |
| 40 | 20 | 20 | 13.57 | 2.89 | 5.78 | 1.90 | 5.40 | 1.26 | 4.26 | 1.62 |
| 40 | 20 | 30 | 13.87 | 2.10 | 2.20 | 0.12 | 2.50 | 0.25 | 2.79 | 0.37 |
| 40 | 40 | 10 | 17.56 | 1.53 | 4.63 | 0.48 | 4.84 | 0.77 | 6.85 | 0.73 |
| 40 | 40 | 20 | 14.42 | 2.16 | 2.32 | 0.18 | 2.47 | 0.20 | 2.98 | 0.29 |
| 40 | 40 | 30 | 11.66 | 2.21 | 1.90 | 0.10 | 2.44 | 0.50 | 2.44 | 0.31 |
| 40 | 40 | 40 | 12.80 | 4.07 | 3.04 | 0.64 | 2.80 | 0.47 | 2.80 | 0.82 |
| 40 | 40 | 50 | 9.05 | 1.11 | 2.47 | 0.53 | 2.24 | 0.26 | 3.05 | 0.78 |
| 40 | 40 | 60 | 7.82 | 0.80 | 2.51 | 0.68 | 2.23 | 0.28 | 3.28 | 1.01 |
| 40 | 60 | 10 | 16.27 | 1.95 | 3.48 | 0.34 | 3.53 | 0.44 | 4.84 | 0.66 |
| 40 | 60 | 20 | 12.23 | 2.23 | 2.19 | 0.13 | 2.39 | 0.18 | 2.94 | 0.26 |
| 40 | 60 | 30 | 14.40 | 3.99 | 1.84 | 0.12 | 2.13 | 0.30 | 2.12 | 0.18 |
| 40 | 60 | 40 | 13.57 | 4.06 | 5.05 | 1.18 | 3.36 | 0.64 | 6.01 | 2.03 |
| 40 | 60 | 50 | 7.56 | 0.94 | 3.24 | 0.92 | 2.43 | 0.43 | 4.04 | 0.90 |
| 40 | 60 | 60 | 10.01 | 2.86 | 3.45 | 1.08 | 2.83 | 0.71 | 3.13 | 0.87 |
| 40 | 60 | 70 | 16.88 | 6.16 | 7.02 | 1.30 | 4.88 | 0.96 | 7.21 | 1.47 |
| 50 | 40 | 10 | 16.24 | 1.59 | 2.61 | 0.23 | 2.69 | 0.22 | 4.03 | 0.53 |
| 50 | 40 | 20 | 11.71 | 1.47 | 1.94 | 0.11 | 2.23 | 0.09 | 3.19 | 0.61 |
| 50 | 40 | 30 | 12.46 | 1.16 | 2.38 | 0.18 | 2.77 | 0.12 | 3.62 | 0.30 |
| 50 | 40 | 40 | 12.16 | 1.43 | 2.40 | 0.41 | 2.90 | 0.17 | 3.38 | 0.35 |
| 50 | 60 | 10 | 17.75 | 1.71 | 4.07 | 0.25 | 3.93 | 0.42 | 5.71 | 0.64 |

Table 6.1 Continued Visualization study results

| | | | | | | | | | | |
|---|---|---|---|---|---|---|---|---|---|---|
| 50 | 60 | 20 | 14.82 | 1.75 | 2.92 | 0.25 | 3.18 | 0.18 | 4.52 | 0.84 |
| 50 | 60 | 30 | 12.65 | 1.21 | 2.64 | 0.27 | 2.95 | 0.21 | 3.89 | 0.58 |
| 50 | 60 | 40 | 9.65 | 1.38 | 2.12 | 0.07 | 2.52 | 0.06 | 3.11 | 0.32 |
| 50 | 60 | 50 | 9.94 | 0.97 | 2.12 | 0.08 | 2.55 | 0.09 | 2.96 | 0.18 |
| 50 | 60 | 60 | 8.85 | 0.41 | 3.77 | 1.24 | 3.27 | 0.63 | 3.66 | 0.99 |
| 50 | 60 | 70 | 10.70 | 3.32 | 11.18 | 2.16 | 7.72 | 1.54 | 12.41 | 2.48 |
| 60 | 40 | 10 | 16.16 | 1.82 | 3.13 | 0.30 | 2.87 | 0.15 | 5.09 | 0.82 |
| 60 | 40 | 20 | 9.79 | 1.51 | 2.15 | 0.11 | 2.36 | 0.07 | 2.60 | 0.12 |
| 60 | 60 | 10 | 14.85 | 2.00 | 3.79 | 0.37 | 3.33 | 0.23 | 6.59 | 1.06 |
| 60 | 60 | 20 | 11.44 | 1.30 | 2.19 | 0.15 | 2.30 | 0.08 | 3.14 | 0.35 |
| 60 | 60 | 30 | 9.95 | 1.13 | 1.96 | 0.16 | 2.15 | 0.10 | 2.36 | 0.13 |
| 70 | 60 | 10 | 13.62 | 1.36 | 3.02 | 0.24 | 2.68 | 0.13 | 4.69 | 0.64 |
| 70 | 60 | 20 | 9.99 | 1.16 | 1.95 | 0.08 | 2.14 | 0.06 | 2.72 | 0.25 |
| 80 | 60 | 10 | 11.56 | 1.40 | 2.60 | 0.17 | 2.42 | 0.09 | 3.92 | 0.41 |